

## Magnetic Interfaces and Nanostructures Room 121 - Session MI+2D+AC+TF-WeM

### Altermagnetism and Spin-Dependent Systems

**Moderators:** Markus Donath, Muenster University, Germany, Valeria Lauter, Oak Ridge National Laboratory

8:00am **MI+2D+AC+TF-WeM-1 Twisted Electrons in Momentum Space: A Photoemission Perspective on Spin and Orbital Angular Momentum in Quantum Materials**, Maximilian Ünzelmann, University of Würzburg, Germany; B. Geldiyev, University of Würzburg, Germany; T. Figgemeier, University of Würzburg, Germany; H. Bentmann, NTNU Trondheim, Norway; F. Reinert, University of Würzburg, Germany

**INVITED**

Beyond the spin, electronic states in crystalline solids can exhibit finite expectation values of orbital angular momentum (OAM). This phenomenon has attracted considerable attention in recent years and can particularly be traced back to the following key applications: (i) Since OAM is formed solely by inversion symmetry breaking (ISB) – and thus can also be present without magnetism or strong spin-orbit coupling (SOC) – it appears as an interesting quantum degree of freedom raising the potential of orbital analogs to spintronic phenomena, i.e. the field of *orbitronics*. (ii) OAM has been proposed to be a useful observable to assess nontrivial topology in the band structure of topological quantum matter. Lastly, if the atomic SOC strength is sizable, OAM is coupled to the electron spin giving rise to rich spin and orbital momentum space textures.

In this talk, I will shed light on those textures from the perspective of angle-resolved photoemission spectroscopy (ARPES). Combining ARPES with light-polarization-dependent and spin-resolved measurements allows us to address the momentum-dependent properties of the spatial and spin part of the wave functions, respectively. I will present experimental results on model-like monolayer systems and topological quantum materials and show that – as well as how – the complex interplay of ISB and SOC forms striking spin-orbital textures. Based on these findings, I will discuss the potential of utilizing OAM (i) towards orbitronic transport and (ii) to detect unexpected topological features.

8:30am **MI+2D+AC+TF-WeM-3 Falicov Student Award Finalist Talk: Gap Tuning by Hole Doping in EuZn<sub>2</sub>As<sub>2</sub> Semimetal**, Dejia Kong<sup>1</sup>, University of Virginia; S. Karbasizadeh, University of South Carolina; G. Narasimha, Oak Ridge National Laboratory; P. Regmi, University of South Carolina; C. Tao, Oak Ridge National Laboratory; S. Mu, University of South Carolina; R. Vasudevan, Oak Ridge National Laboratory; I. Harrison, University of Virginia; R. Jin, University of South Carolina; Z. Gai, Oak Ridge National Laboratory

EuZn<sub>2</sub>As<sub>2</sub> is an ideal candidate for topological magnetism study in comparison to other europium-based semimetals that exhibit a similar type of magnetic transition from the antiferromagnetic phase to the ferromagnetic phase at a low temperature. <sup>1</sup> Theoretical calculations predict gapped and flatter bands in EuZn<sub>2</sub>As<sub>2</sub> but a gapless  $\Gamma$  point in EuCd<sub>2</sub>As<sub>2</sub>. <sup>2</sup> In this work, a low-temperature cleaved EuZn<sub>2</sub>As<sub>2</sub> crystal is studied using scanning tunneling microscopy/spectroscopy (STM/S) and density functional theory (DFT). A group of triangular-shaped defects in combining with the DFT calculations are used to identify the existence of the europium-terminated and arsenic-terminated surfaces at the cleavage. Large bandgaps are observed on the two pristine terminations. However, the bandgap width is found to be very sensitive to local heterogenous, like defects and step edges. Two defect groups that create local electron deficiency, i.e. substitutional defect of As replacing Zn, and Zn vacancy, can drastically lower the bandgap. Furthermore, the modification of the bandgap width shows a discrepancy on the two terminations, bigger on Eu termination but much smaller on As-Zn termination. So, we predict that purposely hole doping the system during the crystal growth stage may create a new topological semimetal material with a gapless europium layer sandwiched by a gapped As-Zn lattice.

Reference:

<sup>1</sup> Blawat, J. *et al.* Unusual Electrical and Magnetic Properties in Layered EuZn<sub>2</sub>As<sub>2</sub>. *Adv Quantum Technol* **5** (2022).

<sup>2</sup> Wang, Z. C. *et al.* Anisotropy of the magnetic and transport properties of EuZn<sub>2</sub>As<sub>2</sub>. *Phys Rev B* **105** (2022).

8:45am **MI+2D+AC+TF-WeM-4 Characterization of LaMnO<sub>3</sub>/SrTiO<sub>3</sub> Thin Films and Its Mn Valence State Correlated with Ferromagnetism**, Ghadendra Bhandari, P. Tavazohi, V. Dewasurendra, M. Johnson, M. Holcomb, West Virginia University

Thin films of LaMnO<sub>3</sub> (LMO) / SrTiO<sub>3</sub> (STO) perovskite have gained interest for their abilities to be an essential component of some heterostructures while still exhibiting an interesting magnetic phase diagram. We have grown LaMnO<sub>3</sub> thin films on SrTiO<sub>3</sub> using pulsed laser deposition and deposition has been monitored by reflection high energy electron diffraction (RHEED) to verify layer-by-layer growth. Structure and magnetic properties have been characterized by X-ray diffractometry (XRD), and vibration sample magnetometry (VSM). LaMnO<sub>3</sub> thin films exhibit ferromagnetic FM phases whereas bulk LaMnO<sub>3</sub> is antiferromagnetic A-type. All thin films are coherently strained, forcing them to have the in-plane lattice parameter of the STO substrate (3.905 Å), but the out-of-plane parameter varies (3.89-3.93 Å). The variation in the c-lattice is developed from O<sub>2</sub> growth pressure and consequently the Mn cation is in mixed valence state Mn<sup>3+/4+</sup>. The valence state of the Mn cation is realized from XPS and XAS study. The ferromagnetic magnetization is originated by the double exchange of Mn<sup>3+</sup>-O-Mn<sup>4+</sup>. The thickness averaged magnetizations from PNR measurements are comparable with magnetization obtained from VSM. The strength of magnetization correlates with content of Mn<sup>4+</sup>.

9:00am **MI+2D+AC+TF-WeM-5 Altermagnetism: From Spintronics to Unconventional Magnetic Phases**, Libor Šmejkal, Uni Mainz, Germany

**INVITED**

The search for unconventional quantum phases that break the symmetries of the crystal lattice has been a focus in physics since the early days of quantum theory, driven by both fundamental interest and potential applications. Prominent examples include cuprate superconductors, which are known for their unconventional d-wave Cooper pairing, and dissipationless transport.

In this presentation, we will discuss our recent discovery<sup>[1]</sup> of an unconventional magnetic phase motivated by our earlier predictions and observations of unconventional spintronics effects <sup>[2,3,4]</sup>. This unconventional phase, altermagnetism (see Figure), unlike common ferromagnetism and antiferromagnetism, breaks the symmetries of the crystal lattice, and features d, g, or i-partial wave characteristics simultaneously in its spin and electronic structure<sup>[1]</sup>. D-wave altermagnetism thus represents magnetic analogue of d-wave superconductivity.

We identified altermagnetism by employing and developing a symmetry framework that considers paired transformations involving electron spin and the crystal lattice. This framework is emerging as a new paradigm in the study of magnetic crystals. We will demonstrate its usefulness by discussing (i) the altermagnetic band structure of the semiconductor MnTe, which we recently experimentally observed through collaborative work using photoemission spectroscopy<sup>[5]</sup>, and (ii) our identification of more than 240 realistic altermagnetic candidates.

Additionally, we will explore the rapid expansion of altermagnetic concepts to many fields with focus on ultrafast spintronics memories<sup>[6]</sup>, dissipationless transport <sup>[2-4]</sup> and two-dimensional band topology <sup>[7]</sup>. Finally, we will outline the latest developments in the field, including the theoretical identification of the magnetic analog of superfluid helium-3 and we will propose transport experiments which can be used for its detection<sup>[8]</sup>.

[1] L. Šmejkal, J. Sinova, and T. Jungwirth, *Phys. Rev. X* **12**, 031042 (2022)

[2] L. Šmejkal, et al., *Sci. Adv.* **6**, eaaz8809 (2020)

[3] I. Mazin, et al., *PNAS* **118**, e2108924118 (2021)

[4] H. Reichlová, et al., *Nature Communications* **15**, 4961 (2024)

[5] J. Krempasky\*, L. Šmejkal\*, S. Souza\*, et al., *Nature*, **626**, 517 (2024)

[6] L. Šmejkal et al., *Phys. Rev. X* **12**, 011028 (2022)

[7] I. Mazin, R. Gonzalez-Hernandez, and L. Šmejkal, arXiv:2309.02355 (2023)

[8] Birk Hellenes, et al., arXiv:2309.01607v2 (2024)

# Wednesday Morning, November 6, 2024

9:30am **MI+2D+AC+TF-WeM-7 Growth Study of Kagome-structured Mn<sub>3</sub>Sn on Gallium Nitride (000-1) Using Molecular Beam Epitaxy**, *H. Hall, S. Upadhyay, T. Erickson, A. Shrestha, A. Abbas, Arthur Smith*, Ohio University  
Over the past few years, there has been a large amount of interest in Kagome-structured magnetic materials with non-collinear antiferromagnetic ordering [1]. Such materials show interesting magnetic properties including anomalous Hall effect and topological Hall effect [2]. In recent work, we have reported growth of Mn<sub>3</sub>Sn on sapphire (0001) which resulted in either *a*-plane or *c*-plane film orientations [3,4]. The substrate however was not ideal, and frequently we observed the disappearance of the diffraction pattern upon opening the Mn and Sn shutters with the pattern reappearing after some amount of resting time. In the case of the *c*-plane orientation, theory suggested this could be due to interfacial disordering of the lattice. This might be due to the ~19% lattice mismatch which also is one reason for the preferred growth of *a*-plane oriented Mn<sub>3</sub>Sn on sapphire (0001) due to the much smaller lattice mismatch (<5%) along that direction. Nonetheless, high quality films prove difficult to obtain on sapphire (0001), and a better substrate is desirable. As such, we have investigated the growth of Mn<sub>3</sub>Sn films on freshly grown gallium nitride surfaces. The Mn<sub>3</sub>Sn growth follows immediately after the growth of N-polar GaN (000 $\bar{1}$ ), thus giving a perfectly clean and well-ordered substrate surface with only ~2.66% lattice mismatch along the 30° line to the high symmetry axis of GaN. We have investigated this as a function of substrate temperature and find an optimal temperature range in which streaky and clear RHEED patterns are obtained from the beginning of the growth. Next plans include studying of this surface with high-resolution STM and spin-polarized STM. This research has been supported by the U.S. Department of Energy, Office of Basic Energy Sciences, Division of Materials Sciences and Engineering under Award No. DE-FG02-06ER46317.

- [1] H. Yang *et al.*, *New J. of Physics* **19**, 015008 (2017).  
[2] S. Nakatsujii, N. Kiyohara, and T. Higo, *Nature* **527**, 212 (2015).  
[3] S. Upadhyay *et al.*, *J. Vac. Sci. & Technol. A* **41**, 042710 (2023).  
[4] S. Upadhyay *et al.*, *Surfaces and Interfaces* **42**, 103379 (2023).

9:45am **MI+2D+AC+TF-WeM-8 Exchange Bias Effect in Single-Layer Antiferromagnetic Mn<sub>3</sub>GaN Films**, *Ali Abbas, A. Shrestha*, Ohio University; *D. Russell, F. Yang*, The Ohio State University; *A. Smith*, Ohio University  
Strain-induced spin structures in non-collinear antiferromagnetic materials like Mn<sub>3</sub>GaN can be controlled by an external magnetic field[1][2]. In this work, we report the intrinsic exchange bias in the “single” antiferromagnetic Mn<sub>3</sub>GaN films fabricated by epitaxial growth of Mn<sub>3</sub>GaN on MgO (001) substrate using molecular beam epitaxy under *in-plane* tensile and *out-of-plane* compressive strain. Scanning transmission electron microscopy confirms significant strain at the Mn<sub>3</sub>GaN/MgO interface due to substrate induced tetragonal distortion. Superconducting quantum interference device measurements reveal an exchange bias field (H<sub>eb</sub>=1225 Oe) and a vertical magnetization shift below 300 K. Furthermore, magnetization M vs. the applied field H measurements from 300K down to 50K reveal the consistent horizontal and vertical shift of the hysteresis loop, which are usually observed only in ferro-/antiferromagnetic bilayers. Here, the exchange bias effect may be attributed to strain, leading to canted and uncompensated Mn spins coupled with an upper antiferromagnetic region, as reported in another system [2][3]. The findings of strain-induced exchange bias in antiferromagnetic Mn<sub>3</sub>GaN films may open a new route/ novel system for spintronic properties by design. This research has been supported by the U.S. Department of Energy, Office of Basic Energy Sciences, Division of Materials Sciences and Engineering under Award No. DE-FG02-06ER46317 (work done at Ohio University, not including XRD) and under award No. DE-SC0001304 (XRD and SQUID measurements done at The Ohio State University).

References:

- [1] X.F. Zhou *et al.*, “Exchange Bias in Antiferromagnetic Mn<sub>3</sub>Sn Monolayer Films,” *Physical Review Applied*, 14(5), 054037 (2020).  
[2] B. Cui *et al.*, “Strain engineering induced interfacial self-assembly and intrinsic exchange bias in a manganite perovskite film”. *Scientific reports*, 3(1), 2542, (2013).  
[3] L. Wanget *et al.*, “Exchange bias and vertical shift of the magnetic hysteresis loop in Co/BiFeO<sub>3</sub> bilayers. *Ferroelectrics Letters Section*, 48(4–6), 65–71, (2021).

11:00am **MI+2D+AC+TF-WeM-13 L-Gap Surface Resonance at Pt(111): Influence of Atomic Structure, d Bands, and Spin-Orbit Interaction**, *Markus Donath, F. Schöttke, P. Krüger*, University of Münster, Germany; *L. Hammer, T. Kiblinger, M. Schneider*, University of Erlangen-Nürnberg, Germany

Pt(111) hosts a surface resonance with peculiar properties concerning energy vs momentum dispersion and spin texture. At variance with the free-electronlike behavior of the L-gap Shockley-type surface states on the fcc(111) surfaces of Au, Ag, and Cu, it splits into several branches with distinct spin polarization around the center of the surface Brillouin zone. Theoretical predictions based on density-functional theory vary depending on the particular functionals used. To clarify this issue, we investigate the atomic structure of Pt(111) by low-energy electron diffraction and the unoccupied electronic structure by spin- and angle-resolved inverse photoemission. The experimental results are backed by theoretical studies using different functionals which show that the characteristics of the surface band depend critically on the lattice constant. We identified a delicate interplay of several contributions: Lattice constant, hybridization with d bands, and the influence of spin-orbit interaction are critical ingredients for understanding the peculiar energy dispersion and spin character of the unoccupied surface resonance.

11:15am **MI+2D+AC+TF-WeM-14 Substrate-Induced Strain Effects on SrFeO<sub>3</sub> Thin Films**, *Lucas Barreto*, University of Pennsylvania; *P. Rogge, J. Wang, B. Lefler*, Drexel University; *D. Puggioni, J. Rondinelli*, Northwestern University; *S. Koroluk, R. Green*, University of Saskatchewan, Canada; *S. May*, Drexel University

Materials with non-trivial magnetic ordering give rise to exotic topological phenomena that can enhance spin-based devices' performance. In this scenario, the cubic perovskite SrFeO<sub>3</sub> exhibits a rich magnetic ordering, described by a multi-*q* magnetic arrangement. In this work, we evaluate how in-plane lattice stress influences the structural, magnetic, and electronic of SrFeO<sub>3</sub> films. We grow epitaxial SrFeO<sub>3</sub> films on different substrates to induce compressive and tensile strains, characterize them using X-ray diffraction, and probe the electronic transport as a function of temperature. The experimental data are supported by density functional theory calculations, from which we obtain the structural and electronic properties of the strained SrFeO<sub>3</sub> structure. We map the magnetic ordering via resonant x-ray magnetic diffraction and observe shifts in the projection of the magnetic wavevector *q* along the [111] direction. Our results indicate that the lattice strain can tune the magnetic propagation vector on the films while maintaining the SrFeO<sub>3</sub> metallic behavior.

11:30am **MI+2D+AC+TF-WeM-15 Tunable Localized Currents at Crystallographic Domain Boundaries in Altermagnet RuO<sub>2</sub>**, *Gina Pantano, E. Thareja*, University of South Florida; *L. Šmejkal*, the Czech Academy of Sciences and Johannes Gutenberg Universität Mainz, Germany; *J. Sinova, Johannes Gutenberg Universität Mainz, Germany; J. Gayles*, University of South Florida

Research on interfacial phenomena in condensed matter physics has garnered significant interest over the last few decades due to the discovery of new properties and phases distinct from the bulk, enabling the manipulation of materials for technological applications. In this work, we investigate the novel effects that arise from the presence of a locally chiral crystallographic domain boundary in the altermagnet ruthenium dioxide (RuO<sub>2</sub>). Altermagnets are characterized by having a substantial non-relativistic spin splitting comparable to ferromagnetic materials but with compensated magnetic ordering. The spin splitting originates from the Heisenberg exchange interaction combined with the anisotropic octahedral crystal field from the surrounding nonmagnetic O atoms, which reduces the symmetry relating the two opposite spin sublattices to an antiunitary rotation or mirror symmetry. This introduces a new mechanism for controlling spin-dependent transport phenomena by altering the crystal configuration, specifically through its local chirality, such as the crystal Hall effect. Thus, looking at an interface where the local chirality reverses allowed for a more detailed analysis of how the change of symmetry affects electronic transport. RuO<sub>2</sub> was chosen for this study due to its high Néel temperature, metallic nature, and exhibiting one of the largest spin splittings in this new material class. We use first-principle calculations to characterize the interfacial states and their contribution to electronic transport. We observe an induced magnetization at the domain boundary and enhanced anomalous transport along the interface when spin-orbit coupling is considered, due to the change of symmetry. We theorize the localized currents are tunable by the direction of the magnetization at the interface. Our findings will contribute to the understanding of how altermagnetic properties evolve toward interfaces with the reduction in

# Wednesday Morning, November 6, 2024

dimensionality and symmetry and contribute to advancements toward the design of sustainable, energy-efficient devices.

## Magnetic Interfaces and Nanostructures

Room 121 - Session MI+2D+AC+TF-WeA

### 2D Magnetism and Magnetic Nanostructures

Moderators: Mikel Holcomb, West Virginia University, Tiffany Kaspar, Pacific Northwest National Laboratory

2:15pm MI+2D+AC+TF-WeA-1 Interface Tunable Magnetism in Transition Metal Telluride Thin Films and Heterostructures, *Hang Chi*, University of Ottawa, Canada

INVITED

Novel quasi-2D magnets are attracting much attention recently. In situ prepared sharp interfaces are desirable for strain engineering and/or hybridizing with other quantum systems, enabling fundamentally new phenomena and opportunities for spintronics [1]. Ferromagnetic Cr<sub>2</sub>Te<sub>3</sub> ultrathin films, optimally grown on Al<sub>2</sub>O<sub>3</sub>(0001) and SrTiO<sub>3</sub>(111) using molecular beam epitaxy, manifest an extraordinary sign reversal in the anomalous Hall conductivity as temperature and/or strain are modulated. The nontrivial Berry curvature in the electronic-structure momentum space is believed to be responsible for this behavior [2]. Furthermore, when proximitized with (Bi,Sb)<sub>2</sub>Te<sub>3</sub>-type topological insulator, via the Bloembergen-Rowland interaction, magnetic ordering in monolayer Cr<sub>2</sub>Te<sub>3</sub> is favorably enhanced, displaying an increased Curie temperature [3]. Combining ab initio simulation, advanced scanning tunneling microscopy, magnetic force microscopy, transmission electron microscopy, magneto transport and particularly depth-sensitive polarized neutron reflectometry, Cr<sub>2</sub>Te<sub>3</sub> has been established as a far-reaching platform for further investigating the marriage of magnetism and topology. These findings provide new perspectives to the magnetic topological materials in general, that are topical for the future development of topological spintronics.

#### References

- [1] H. Chi and J. S. Moodera, "Progress and prospects in the quantum anomalous Hall effect", *APL Mater.* **10**, 090903 (2022). <https://doi.org/10.1063/5.0100989>
- [2] H. Chi, Y. Ou, T. B. Eldred, W. Gao, S. Kwon, J. Murray, M. Dreyer, R. E. Butera, . . . J. S. Moodera, "Strain-tunable Berry curvature in quasi-two-dimensional chromium telluride", *Nat. Commun.* **14**, 3222 (2023). <https://doi.org/10.1038/s41467-023-38995-4>
- [3] Y. Ou, M. Mirzhalilov, N. M. Nemes, J. L. Martinez, M. Rocci, A. Akey, W. Ge, D. Suri, . . . H. Chi, "Enhanced Ferromagnetism in Monolayer Cr<sub>2</sub>Te<sub>3</sub> via Topological Insulator Coupling", *arXiv:2312.15028* (2024). <https://doi.org/10.48550/arXiv.2312.15028>

#### Acknowledgment

We acknowledge the support of the Natural Sciences and Engineering Research Council of Canada (NSERC) Discovery Grant RGPIN-2024-06497.

2:45pm MI+2D+AC+TF-WeA-3 AVS National Student Awardee Talk/Falicov Student Award Finalist Talk: Probing Intrinsic Magnetization Dynamics of the Y<sub>3</sub>Fe<sub>5</sub>O<sub>12</sub>/Bi<sub>2</sub>Te<sub>3</sub> Interface at Low Temperature, *A. Willcole*, Sandia National Laboratories, USA; *V. Lauter*, Oak Ridge National Laboratory, USA; *A. Grutter*, National Institute of Standards and Technology (NIST); *C. Dubs*, INNOVENT e.V. Technologieentwicklung, Germany; *D. Lidsky*, Sandia National Laboratories, USA; *Bin Luo*<sup>1,2</sup>, Northeastern University, US; *M. Lindner*, *T. Reimann*, INNOVENT e.V. Technologieentwicklung, Germany; *N. Bhattacharjee*, Northeastern University, US; *T. Lu*, *P. Sharma*, *N. Valdez*, *C. Pearce*, *T. Manson*, Sandia National Laboratories, USA; *M. Matzelle*, *A. Bansil*, *D. Heiman*, *N. Sun*, Northeastern University, US

Topological insulator-magnetic insulator (TI-MI) heterostructures are essential in spintronics, enabling magnetization control via topological surface state-induced spin orbit torque. However, many TI-MI interfaces often face issues like contamination in the magnetic insulator and a low-density transitional region in the topological insulator, which obscure the system's intrinsic properties. In this study, we addressed these challenges by depositing sputtered Bi<sub>2</sub>Te<sub>3</sub>(BT) on liquid phase epitaxy grown Y<sub>3</sub>Fe<sub>5</sub>O<sub>12</sub> (YIG)/Gd<sub>3</sub>Ga<sub>5</sub>O<sub>12</sub>. The liquid phase epitaxy grown YIG exhibits exceptional interface quality, without an extended transient layer derived from interdiffusion processes of the substrate or impurity ions, thereby eliminating rare-earth impurity-related losses in the MI at low temperatures. At the TI-MI interface, high resolution depth-sensitive polarized neutron reflectometry confirmed the absence of a low-density transitional growth region of the TI. The demonstrated BT/YIG system is

uniquely suited to elucidate the intrinsic TI-magnetic insulator magnetization dynamics due to the lack of an extended transient layer in the magnetic insulator at the magnetic insulator-substrate interface and lack of a low density, intergrowth region of the TI at the TI-magnetic insulator interface.

By overcoming these undesirable interfacial effects, we isolate and probe the intrinsic low-temperature magnetization dynamics and transport properties of the TI-MI interface. Using temperature dependent ferromagnetic resonance (FMR) we found a strong damping enhancement at low temperature due to the topologically protected Dirac surface states (TSS) in the Bi<sub>2</sub>Te<sub>3</sub> film – a signature of significant spin pumping. Accompanying the damping enhancement, we also observed a large induced in-plane magnetic anisotropy for the BT/YIG heterostructure. We explain this by spin-pumping and spin-momentum locking, due to which the precessing spins of the YIG are forced to align with the spins pumped into the TSS and therefore remain locked in the plane of the BT/YIG interface. The temperature dependence of the magnetotransport which supports the suppression of bulk conduction, and the emergence of weak-antilocalization is consistent with the low temperature enhanced spin pumping in the BT/YIG that we observed, highlighting the interplay between the transport and spin pumping behavior in the TI-MI system. Further study of TI-magnetic insulator interfaces, specifically magnetic insulators with perpendicular magnetic anisotropy, are pertinent to potentially unlock high temperature quantum anomalous hall effect (QAHE) heterostructures, and the next generation of low power spintronics.

3:00pm MI+2D+AC+TF-WeA-4 Falicov Student Award Finalist Talk: Surface Investigation of ε-phase Mn<sub>3</sub>Ga on GaN (0001) Substrate using Scanning Tunneling Microscopy, *Ashok Shrestha*<sup>3</sup>, *A. Abbas*, *D. Ingram*, *A. Smith*, Ohio University

Antiferromagnetic materials have garnered significant attention due to their exotic properties and possible applications in next generation spintronic memory and computing devices [1]. In recent years, research on non-collinear antiferromagnetic materials such as Mn<sub>3</sub>X (X: Ir, Ge, Sn, Ga) has heightened due to non-trivial, topological properties of these materials with unique spin textures [2]. Among these Mn-based antiferromagnets, Mn<sub>3</sub>Ir has been commonly employed for applications [3]. As Ir is an expensive metal, efforts have been made to explore Ir-free antiferromagnets. Particularly, Mn<sub>3</sub>Ga emerges as a promising candidate due to its versatile texture, magnetic ordering, and properties akin to Mn<sub>3</sub>Ir [4]. Among the three distinct phases of Mn<sub>3</sub>Ga, one of the most intriguing yet less explored is the ε-phase (D<sub>019</sub>-Mn<sub>3</sub>Ga), which exhibits anomalous Hall effect and topological Hall effect in distinct temperature ranges [3]. In this presentation, we will delve into the growth and surface studies of a thin film of D<sub>019</sub>-Mn<sub>3</sub>Ga on a Ga polar- GaN (0001) substrate.

We have successfully grown an epitaxial ε-phase Mn<sub>3</sub>Ga layer using molecular beam epitaxy. The sample quality, lattice constants and crystal structure of the grown film were determined by *in-situ* reflection high energy electron diffraction and *ex-situ* X-ray diffraction. Upon examination with scanning tunneling microscopy, the surface revealed multiple terraces and row-like structures. Notably, the edges of the terraces form 120° angles with each other, consistent with the hexagonal crystal structure of the ε-phase Mn<sub>3</sub>Ga. Additionally, we observed several stackings of just a monolayer, with their heights matching the *c*/2 value of Mn<sub>3</sub>Ga. These measurements are further confirmed by X-ray diffraction. At atomic resolution, hexagonally arranged atoms with a 1 × 1 crystal structure were observed. The measured average *in-plane* atomic spacing was 5.37 ± 0.05 Å, deviating only -0.56% from theoretical predictions (5.40 Å). However, atomic spacing exhibited local variations. Other interesting structures were also observed in the scanning tunneling microscopy images, which will be discussed in the presentation. Chemical analysis via Rutherford backscattering confirmed the sample's Mn:Ga ratio as 3.2:1.0, which depends on the growth temperature. Further research will involve exploring non-collinear antiferromagnetism using spin-polarized scanning tunneling microscopy, with results to be presented at the conference.

#### References:

- Chen et al., *APL Mater.* **11**, 111026 (2023).  
Qin et al., *Nature* **613**(7944), 48 (2023).  
Hernandez et al., *Surf. and Interface* **41**, 103167 (2023).  
1. Liu et al., *Sci. Rep.* **7**(1), 515 (2017).

<sup>3</sup> Falicov Student Award Finalist

<sup>1</sup> AVS National Student Awardee

<sup>2</sup> Falicov Student Award Finalist

# Wednesday Afternoon, November 6, 2024

## 3:15pm MI+2D+AC+TF-WeA-5 Thermally Generated Spin Transport Across Magnetic Interfaces, *Hari Srikanth*, USF Tampa INVITED

Spin-heat coupling and thermo-spin transport are topical areas of interest for the spintronics community. The origin of longitudinal Spin Seebeck effect (LSSE) and its relationship with magnetic anisotropy as well as magnon propagation across magnetic insulator/heavy metal interfaces have remained challenging issues. LSSE induces incoherent magnon excitations with the application of a temperature gradient across the thickness of a magnetic material. Although the ferrimagnetic insulator  $Y_3Fe_5O_{12}$  (YIG) is known as the benchmark system for LSSE, other members of the insulating rare earth iron garnet family, e.g. the compensated ferrimagnet  $Gd_3Fe_5O_{12}$  (GdIG), ferrimagnetic insulator  $Tm_3Fe_5O_{12}$  (TmIG) etc., are of interest and have received less attention from the point of view of spin-caloritronics. We have pioneered the technique of RF transverse susceptibility to probe the effective magnetic anisotropy in magnetic materials and heterostructures. Combining the RF transverse susceptibility with LSSE measurements, we have shown correlation between bulk and surface anisotropy with the field and temperature dependence of LSSE in YIG/Pt heterostructures and other compensated ferrimagnets like GdIG. Our recent work on TmIG/Pt heterostructures with varying film thickness reveals the clear role of anisotropy and Gilbert damping on the LSSE. From RF susceptibility, LSSE and broadband FMR experiments, quantitative analysis of the magnon propagation length and its correlation with magnetic anisotropy and Gilbert damping has been done. Overall, this talk would present new results in the thermal spin transport of garnet heterostructures which are of fundamental importance in spin transport across magnetic interfaces.

## 4:15pm MI+2D+AC+TF-WeA-9 Spin Switchable 2D-Superlattice Metal-Halide Perovskite Film via Multiferroic Interface Coupling, *Bogdan Dryzhakov*, Oak Ridge National Laboratory; *B. Hu*, University of Tennessee Knoxville; *V. Lauter*, Oak Ridge National Laboratory

Solution-processible 2D-phase metal-halide perovskites have emerged as a remarkable class of semiconducting, exhibiting a wide-range of optoelectronic properties and multi-functionalities. In this work, interfacing ferromagnetic spins with this semiconductor's Rashba band yields magnetic field control over the excited state spin degrees of freedom, as demonstrated through optical analogues that resolve the spin polarization in steady-state and dynamics, and in-situ neutron scattering methods, where a photo-ferromagnetic profile is depth-resolved. The 2D-superlattice perovskite films are prepared using an optimized, low-cost spin-cast method, resulting in highly crystalline and smooth thin films with a well-defined alternating layered structure of self-assembled organic cations and lead-iodide octahedra. Within the anisotropic 2D-planes of MHPs, fluorinated A-site ligands distort the lattice, yielding robust ferroelectricity and Rashba bands arising from broken inversion symmetry and strong spin-orbit coupling. Spin-switchable circularly polarized photoluminescence (CPL) between  $\sigma^+$  and  $\sigma^-$  polarizations is achieved at the multiferroic perovskite/Co interface by manipulating the ferromagnetic spins on the Co surface between positive and negative magnetic field directions. This switching behavior arises from selective interactions between the ferromagnetic spins on the Co surface and the circularly polarized  $\sigma^+$  and  $\sigma^-$  orbitals within the perovskite's Rashba band structures. Polarized neutron reflectometry measurements reveal long-range interactions of the Co magnetism to the perovskite's spin-polarized excitons, with chemical (NSLD) and magnetization (MSLD) depth profiles indicating optically induced magnetization through the perovskite's thickness. This work presents a fundamental platform for exploring spin selectivity effects within Rashba band structures using CPL studies in multiferroic perovskite/ferromagnetic interfaces.

## 4:30pm MI+2D+AC+TF-WeA-10 Engineering the Hybrid Nanocolumnar Metamaterial Platforms for Advanced Optical and Magnetic Applications, *Ufuk Kilic*, *C. Briley*, University of Nebraska-Lincoln; *R. Feder*, Fraunhofer Institute for Microstructure of Materials and Systems, Germany; *D. Sekora*, University of Nebraska-Lincoln; *A. Ullah*, University of Nebraska - Lincoln; *A. Mock*, Weber State University; *C. Binek*, University of Nebraska - Lincoln; *H. Schmidt*, Friedrich Schiller University, Germany; *C. Argyropoulos*, The Pennsylvania State University; *E. Schubert*, *M. Schubert*, University of Nebraska - Lincoln

The hybrid metamaterial platforms have garnered remarkable attention in various subdisciplines of physics, chemistry, and biology due to their wide range of advanced functionalities including strong tunable optical and magnetic anisotropies, the ability to confine, modulate, and control of light, to engineer new permanent nanomagnets, for example. In this study, we employed a custom-built ultra-high vacuum electron-beam glancing angle deposition technique [1] to fabricate spatially-coherent, super lattice type

nanocolumnar heterostructure metamaterial platforms from both hard (cobalt) and soft (permalloy) magnetic materials. Furthermore, by using atomic layer deposition technique, we incorporate ultrathin interface layer (~1.4 nm) of  $Al_2O_3$  between the magnetic nano-columnar subsegments. This interface engineering at nanoscale provides another angle of freedom to tune both the magnetic and optical properties of hybrid nanocolumnar metamaterial platforms.

By taking the advantage of the generalized spectroscopic ellipsometry technique, we reached out the complex anisotropic dielectric properties of the fabricated structures. Our analysis involves widely used anisotropic Bruggeman effective medium model approach which provides to extract optical and structural properties, accordingly [2]. Moreover, to perform magnetic characterization of our fabricated metamaterial design, we employed both generalized vector magneto-optic ellipsometry and vibrating sample magnetometer measurements [3]. In order to delve into the fundamental driving mechanisms behind the anisotropic tunable magneto-optic responses from the proposed metamaterial platforms, we conducted a series of systematic micromagnetic and finite element modeling simulations, as well. We believe that these new structural metamaterial designs can result in the development of next-generation sensing devices, permanent nanomagnets, magnetic recording technologies, on-chip nanophotonic and opto-magnetic device applications.

References:

- [1] Kilic, U., et al. *Sci Rep* 9, 71 (2019).
- [2] Schmidt, D., and Schubert, M., *J. Appl. Phys.* 114.8 (2013).
- [3] Briley, Chad, et al. *Appl. Phys. Lett.* 106.13 (2015).

## 4:45pm MI+2D+AC+TF-WeA-11 Magnetic Field Affects Oxygen Evolution Reaction Only in Metal Oxy-Hydroxides, *Filippo Longo*, Chemical Energy Carriers and Vehicle Systems Laboratory, Empa, Swiss Federal Laboratories for Materials Science and Technology, Switzerland; *R. Peremadathil Pradeep*, *E. Darwin*, *H. Hug*, Magnetic and Functional Thin Films Laboratory, Empa, Swiss Federal Laboratories for Materials Science and Technology, Switzerland; *A. Borgschulte*, Chemical Energy Carriers and Vehicle Systems Laboratory, Empa, Swiss Federal Laboratories for Materials Science and Technology, Switzerland

Ni-based electrodes have been largely employed in alkaline electrolyzers for the production of  $H_2$  and  $O_2$  [1]. Due to the sluggish kinetics of the oxygen evolution reaction (OER), many experimental approaches have been employed to boost the catalytic performance of such electrodes [2]. The application of an external magnetic field during OER has shown outstanding catalytic improvement [3]. Despite considerable research effort, the understanding of its origin is still object of debate [4,5]. In this work we show how the Ni-based electrodes improve their catalytic activity towards OER during the application of an external magnetic field. We investigate in detail the catalytically active surface, the microscopic, electronic, and magnetic structures by soft- and hard X-ray photoelectron spectroscopy combined with impedance spectroscopy and magneto-optical measurements. It is relevant in this context that the oxy-hydroxide formed during OER is the catalytically active compound, and is thus likely also the origin of the magnetic effect. To underline the importance of the oxy-hydroxide formation, we employ a multilayered system made of Co-Pt-Ru multi-lattices, exhibiting much more favorable magnetic properties (such as strong perpendicular magnetic anisotropy) than nickel. Interestingly, hardly any improvement of OER is found. The various findings corroborate the picture of spin-exchange interaction of metal-oxide bonds as the underlying mechanism of the magneto-chemical effect.

- [1] S. W. Sharshir et al., *International Journal of Hydrogen Energy* (2023).[2] J. S. Kim et al., *Adv. Energy Mater.* (2018), 8, 1702774.[3] F.A. Garcés-Pineda et al., *Nat Energy* 4, 519–525 (2019).[4] T. Wu et al., *Nat Commun* 12, 3634 (2021).[5] X. Ren et al., *Nat Commun* 14, 2482 (2023).

## Actinides and Rare Earths

### Room 123 - Session AC+MI-ThM

#### Superconductivity, Electron Correlation, Magnetism and Complex Behavior

**Moderators:** Tomasz Durakiewicz, Idaho National Laboratory, Ladislav Havela, Charles University, Czech Republic, David Shuh, Lawrence Berkeley National Laboratory, James G. Tobin, University of Wisconsin-Oshkosh

#### 8:00am AC+MI-ThM-1 Electronic Structures of f-Electron Superconductors, Shin-ichi Fujimori, Japan Atomic Energy Agency, Japan **INVITED**

The unconventional superconductors in *f*-based materials attract much attention in recent years. In the present talk the electronic structures of *f*-electron superconductors UTe<sub>2</sub> and CeIr<sub>3</sub> will be presented.

Recently, it was discovered that UTe<sub>2</sub> has relatively high transition temperature ( $T_c=2.1$  K), and it is classified into one of such class of materials [1,2]. The electronic structure of UTe<sub>2</sub> was studied by resonant photoelectron spectroscopy (RPES) and angle-resolved photoelectron spectroscopy (ARPES) with soft X-ray synchrotron radiation [3]. The partial U 5*f* density of states of UTe<sub>2</sub> were imaged by the U 4*d*-5*f* RPES and it was found that the U 5*f* state has an itinerant character, but there exists an incoherent peak due to the strong electron correlation effects. The band structure of UTe<sub>2</sub> was obtained by ARPES and its overall band structure was mostly explained by band structure calculations, except for the incoherent band at  $E_F \sim 0.5$  eV. These results suggest that the U 5*f* states of UTe<sub>2</sub> have itinerant but strongly-correlated nature.

The electronic structure of the *f*-based superconductor CeIr<sub>3</sub> ( $T_{SC}=3.1$  K) was also studied by photoelectron spectroscopy [4]. The energy distribution of the Ce 4*f* states were revealed by the Ce 3*d*-4*f* RPES. The contribution of the Ce 4*f* states to the density of states (DOS) at the Fermi energy was estimated to be nearly half of that of the Ir 5*d* states, implying that the Ce 4*f* states have a considerable contribution to the DOS at the Fermi energy. These results suggest that CeIr<sub>3</sub> is an *s*-wave-type superconductor with a considerable contribution from the Ce 4*f* states.

Work performed in collaboration with Ikuto Kawasaki, Yukiharu Takeda, Hiroshi Yamagami, Norimasa Sasabe, Yoshiki J Sato, Ai Nakamura, Yusei Shimizu, Arvind Maurya, Yoshiya Homma, Dexin Li, Fuminori Honda, and Dai Aoki.

#### References

- [1] S. Ran *et al.*, Science **365**, 684 (2019).
- [2] D. Aoki *et al.*, J. Phys. Soc. **88**, 043702 (2019).
- [3] S. Fujimori, *et al.*, J. Phys. Soc. Jpn. **88**, 103701 (2019).
- [4] S. Fujimori *et al.*, Electron. Struct. **5**, 045009 (2023).

#### 8:30am AC+MI-ThM-3 RIXS Study of the 5f Configuration in UTe<sub>2</sub>: Low-Energy Excitations, Te<sub>2</sub> Chains and U Dimers, D. Christovam, M. Sundermann, A. Marino, Max Planck Institute for Chemical Physics of Solids, Germany; H. Gretarsson, PETRA III, Deutsches Elektronen-Synchrotron DESY, Germany; B. Keimer, Max Planck Institute for Solid State Research, Germany; A. Gloskovskii, PETRA III, Deutsches Elektronen-Synchrotron DESY, Germany; M. Haverkort, Institute for Theoretical Physics, Heidelberg University, Germany; I. Elfimov, University of British Columbia, Canada; E. Bauer, P. Rosa, Los Alamos National Laboratory; A. Severing, Institute of Physics II, University of Cologne, Germany; Liu Hao Tjeng, Max Planck Institute for Chemical Physics of Solids, Germany **INVITED**

UTe<sub>2</sub> is a recently discovered odd-parity superconductor, emerging as a promising candidate for topological superconductivity [1-3]. A key challenge in understanding its anisotropic properties and their dependence on tuning parameters is finding the appropriate *Ansatz* for describing such a complex electronic system, situated at the border between localization and itinerancy. It is essential to determine the extent to which local physics persists and to identify the governing electronic *f<sup>n</sup>* configuration. Although the latter has been addressed using various methods, a fierce debate remains about whether the main configuration is *f<sup>2</sup>* or *f<sup>3</sup>*.

Discrepancies in determining the dominant *f<sup>n</sup>* configuration are common in uranium-based intermetallics. We argue that this apparent contradiction arises from the challenge of accurately analyzing the spectra, given the complexity associated with the underlying many-body problem and uncertainties in the input model parameters.

In our study, we opt for a newly developed spectroscopic method for U materials, namely resonant inelastic x-ray scattering (RIXS) in the tender x-ray range [4]. Applying this method to UTe<sub>2</sub>, we can unambiguously detect the presence of atomic-like U 5*f*-5*f* low-energy excitations. This establishes the correlated nature of UTe<sub>2</sub> despite the presence of strong covalence and band formation. Moreover, we can also fingerprint the U 5*f<sup>2</sup>* as the main configuration without the need to rely on accurate calculations, thus settling the debate about the 5*f* valence state [5].

The short Te<sub>2</sub>-Te<sub>2</sub> distances, however, seem incompatible with a formal U<sup>4+</sup> valence. We resolve this puzzle by utilizing band structure calculations and photon energy-dependent photoemission. We found that the charge transfer from the 5*p<sub>y</sub>*<sub>||b</sub> band of the Te<sub>2</sub> chain is directed not to the U 5*f* but to the bonding state of the U 6*d<sub>3z<sup>2</sup>-r<sup>2</sup></sub>* orbitals of the U dimer. Notably, these two band states are non-bonding to each other or to other non-5*f* states in the material. Yet, both bands hybridize with the U 5*f*, emphasizing that the description of the physical properties of UTe<sub>2</sub> must include the Te<sub>2</sub> 5*p<sub>y</sub>*<sub>||b</sub> and U 6*d<sub>3z<sup>2</sup>-r<sup>2</sup></sub>* bands plus the 5*f<sup>2</sup>* *Ansatz* [5] These are all very peculiar findings, making UTe<sub>2</sub> a very special material indeed.

- [1] S. Ran *et al.*, Science, **365**(6454), 684–687 (2019).
- [2] D. Aoki *et al.*, J. Phys. Soc. Jpn. **88**(4), 043702 (2019)
- [3] for recent review: S.K. Lewin *et al.*, Rep. Prog. Phys. **86**(11):114501, 2023.
- [4] A. Marino *et al.*, Phys. Rev. B **108**, 045142 (2023)
- [5] D. S. Christovam *et al.*, arXiv 2402.03852 [https://arxiv.org/abs/2402.03852] (2024)

#### 9:00am AC+MI-ThM-5 Incommensurate Antiferromagnetism in UTe<sub>2</sub> Under Pressure, William Knafo, LNCMI, CNRS, France **INVITED**

The discovery of multiple superconducting phases in UTe<sub>2</sub> boosted research on correlated-electron physics [1,2,3,4]. The proximity to a ferromagnetic quantum phase transition was initially proposed as a driving force to triplet-pairing superconductivity [1], and this heavy-fermion paramagnet was rapidly identified as a reference compound to study the interplay between magnetism and unconventional superconductivity with multiple degrees of freedom.

Here, we present neutron diffraction experiments showing that long-range incommensurate antiferromagnetic order is established in UTe<sub>2</sub> under pressure [5]. The propagation vector  $\mathbf{k}_m = (0.07, 0.33, 1)$  of the observed antiferromagnetic phase is close to a wavevector where antiferromagnetic fluctuations have previously been observed at ambient pressure [6,7]. Our work shows that superconductivity in UTe<sub>2</sub> develops in the vicinity of a long-range antiferromagnetic phase, which differs from the initial proposition of a nearby ferromagnetic phase. The nearly-antiferromagnetic nature of UTe<sub>2</sub> at ambient pressure and its relationship with superconductivity will be discussed.

This work was done in collaboration with T. Thebault, P. Manuel, D. Khalyavin, F. Orlandi, E. Ressouche, K. Beauvois, G. Lapertot, K. Kaneko, D. Aoki, D. Braithwaite, G. Knebel, and S. Raymond.

- [1] Ran *et al.*, Science **365**, 684 (2019).
- [2] Knebel *et al.*, J. Phys. Soc. Jpn. **88**, 063707 (2019).
- [3] Braithwaite *et al.*, Commun. Phys. **2**, 147 (2019).
- [4] Ran *et al.*, Nat. Phys. **15**, 1250–1254 (2019).
- [5] Knafo *et al.*, arXiv:2311.05455.
- [6] Duan *et al.*, Phys. Rev. Lett. **125**, 237003 (2020).
- [7] Knafo *et al.*, Phys. Rev. B **104**, L100409 (2021).

#### 9:30am AC+MI-ThM-7 New Spectroscopic Insights into Correlation Effects and Covalency of U 5f Electrons in Uranium Intermetallic Compounds, A. Marino, M. Sundermann, D. Christovam, Max-Planck Institute for Chemical Physics of Solids, Physics of Correlated Matter, Dresden, Germany; H. Gretarsson, DESY/PETRA-III, Hamburg, Germany; B. Keimer, Max-Planck Institute for Solid State Research, Stuttgart, Germany; A. Gloskovskii, DESY/PETRA-III, Hamburg, Germany; J. Kunes, Department of Condensed Matter Physics, Masaryk University, Brno, Czechia; A. Hariki, Department of Physics and Electronics, Osaka Metropolitan University, Osaka, Japan; L. Tjeng, Max-Planck Institute for Chemical Physics of Solids, Physics of Correlated Matter, Dresden, Germany; Andrea Severing, Institute of Physics II, University of Cologne, Cologne, Germany **INVITED**

Uranium intermetallic compounds exhibit a wide range of fascinating physical phenomena that arise from the intricate interplay between atomic-

# Thursday Morning, November 7, 2024

like correlations and band formation of the U 5f electrons. Describing their electronic structure is a challenge, particularly as atomic-like states have remained experimentally inaccessible. Ongoing disputes revolve around the existence of atomic-like states and, if present, around determining which configuration—U 5f<sup>3</sup> or U 5f<sup>2</sup>—provides the Ansatz or starting point for describing the low-energy properties. Furthermore, these correlated compounds exhibit strong intermediate valency, fuelling intense debates about the actual filling of the 5f shell and the degree of covalency.

This presentation introduces two novel and complementary methods: (1) valence band resonant inelastic x-ray scattering (RIXS) using tender x-rays and (2) photon energy-dependent photoelectron spectroscopy (PES & HAXPES) in combination with DFT+DMFT calculations.

**(1) Valence Band RIXS:** Using high-resolution RIXS at the U M-edges (3.5–3.7 keV), we observe low-energy excitations originating from atomic-like multiplet interactions [1]. The excellent signal-to-background ratio and the multiplet structure serve as a unique fingerprint for the U 5f<sup>n</sup> configuration involved, offering clear evidence of the presence of local correlation physics. This method unambiguously determines the dominating configuration [1].

**(2) Combination of DFT+DMFT calculations with soft and hard x-ray photoemission (PES & HAXPES):** The energy dependencies of the photoionization cross-sections allow for the disentanglement of correlated 5f from band-like non-5f spectral contributions, enabling reliable tuning of parameters such as Hund's-*J*, Hubbard-*U<sub>ff</sub>*, and, most importantly, the double counting correction (*m<sub>dc</sub>*) to reproduce valence band spectra. We applied this method to UGa<sub>2</sub> and UB<sub>2</sub>, two model materials representing the extreme ends of the localization-delocalization range. Despite their vastly different properties, we found the mean 5f shell filling to be almost the same. However, crucially, the distribution of uranium 5f configurations contributing to the ground state differs significantly: narrow in 'localized' UGa<sub>2</sub> and almost statistically broad in 'itinerant' UB<sub>2</sub>. This method also reproduces the satellites in the 4f core-level spectra and explains the presence/absence of 5f-5f-multiplet excitations in the RIXS spectra [2].

[1] A. Marino *et al.* Phys. Rev. B, **108** (2023) 045142  
[2] A. Marino, A. Hariki *et al.*, to be published

**11:00am AC+MI-ThM-13 Isotopic Fingerprinting in Nuclear Forensics: Leveraging Aerogel and LEXAN® SSNTD for Enhanced Analysis, R. Babayew, Itzhak Halevy, N. Elgad, Y. Yehuda-Zada, Ben Gurion Uni., Israel; J. Lorincik, Research Centre Řež, Czech Republic, Israel; M. Last, I. Orion, G. Katarivas-Levy, Ben Gurion Uni., Israel; A. Weiss, Faculty of Engineering, Bar Ilan University, Israel**

In nuclear forensics, ensuring the reliability and accuracy of the analysis is paramount. Traditional methods rely heavily on the expertise of trained researchers, leading to variations in results. To address this challenge, we present innovative techniques aimed at automating Fission Track Analysis through advanced image processing algorithms applied to microscope images.

Our research introduces a pioneering approach that leverages Monte Carlo simulations, particularly utilizing the GEANT4 software, to generate synthetic models of fission tracks. By simulating various physical parameters such as thermal neutron flux, fission cross-section, particle size, and radiation time, our Trainer2 software accurately calculates fission tracks on our Lexan detector, producing results akin to real-world scenarios.

Moreover, our methodology integrates trajectory data from the fission products trajectory database, derived from GEANT4 simulations, to generate synthetic models closely resembling actual microscope images. This synthetic bank of images serves as a controlled and versatile dataset for the development of robust image analysis tools. These tools aim to automate the identification of fission track clusters, thus eliminating the need for manual intervention and minimizing the likelihood of human errors.

Our preliminary software for image processing demonstrates promising efficacy in detecting fission track clusters, providing a comprehensive record of fission sites for analysis. By identifying the length of tracks and their distribution, we can determine the source isotope and the density of impurities, thus advancing our understanding of nuclear materials.

Additionally, the software calculates the number of tracks, enhancing the efficiency of data interpretation.

Furthermore, we introduce a novel approach utilizing penetrating fluorescent colors for 3D scanning of detectors, enhancing our ability to investigate fission track stars beyond mere projections.

In conclusion, our research underscores the importance of automating FTA for nuclear safeguards, aiming to minimize human intervention while fortifying the precision and efficiency of nuclear investigations. Through the seamless integration of GEANT4 simulations and advanced image processing algorithms, we envision a future where nuclear forensic analysis is more reliable, accurate and streamlined.

Keywords: Nuclear forensics, Fission Track Analysis, Monte Carlo simulations, GEANT4, Image processing algorithms, Automated analysis, nuclear safeguards.

## References

[1] Rami Babayew *et al.*, Simulation tools for improvement of the fission track analysis method for nuclear forensics (2024), JRNC, 10.1007/s10967-023-09313-5

**11:15am AC+MI-ThM-14 Unusual orders in the heavy-fermion superconductor CeRh<sub>2</sub>As<sub>2</sub>, Gertrud Zwicknagl, TU Braunschweig, Germany**

The heavy-fermion compound CeRh<sub>2</sub>As<sub>2</sub> exhibits a complex phase diagram with rather unusual states at low temperatures. A prominent example is multi-phase superconductivity [1] which seems to develop inside a normal state characterized by itinerant multi-polar order. The present talk focusses on the instabilities of the strongly renormalized Fermi liquid state in the heavy-fermion compound CeRh<sub>2</sub>As<sub>2</sub>. The central focus is the role played by the non-symmorphic lattice structure and the consequences of the Crystalline Electric Field (CEF) which removes the orbital degeneracy of the Ce 4f states. The narrow quasiparticle bands which arise from the Ce-4f degrees of freedom via the Kondo effect are calculated by means of the Renormalized Band (RB) method. We conjecture that the quasi-quartet CEF ground state in combination with pronounced nesting features of the Fermi surface may give rise to ordered states involving multipolar degrees of freedom [2].

## References

1. S. Khim *et al.*, Science 373, 1012 (2021)
2. RevX 12, 011023 (2022)

**11:30am AC+MI-ThM-15 Thermoelectric Properties of Strongly Correlated Compounds NpPd<sub>3</sub> and PuPd<sub>3</sub>, Krzysztof Gofryk, Idaho National Laboratory; J. Griveau, 3DG Joint Research Centre, Directorate G-Nuclear Safety and Security, Germany; K. McEwen, University College London, UK; W. Nellis, Harvard University; J. Smith, Los Alamos National Laboratory**

Actinides are characterized by the coexistence of localized and itinerant (delocalized) 5f-states near the Fermi energy. This dual nature of the 5f electrons leads to many exotic phenomena that are observed in these strongly correlated materials, spanning magnetic ordering, heavy-fermion ground state, unconventional superconductivity, and/or a "non-Fermi liquid" state. The unusual transport properties of the strongly correlated electron systems are related to the formation, near the Fermi level, of a narrow band with a large density of states. Therefore, the Seebeck coefficient in these materials, being proportional to the density of states at the Fermi level, often reaches large values and shows the characteristic temperature dependence [Phys. Rev. B 94, 195117 (2016)]. To explore the influence of electronic correlations on the transport properties in the AnPd<sub>3</sub> system, here we present low-temperature electrical resistivity and Seebeck coefficient measurements of NpPd<sub>3</sub> and PuPd<sub>3</sub> intermetallics. We show that the electrical resistivity shows characteristic behavior of systems with Kondo interactions. The magnitude and overall temperature dependence of the thermoelectric power of NpPd<sub>3</sub> and PuPd<sub>3</sub> are characteristic of 4f- and 5f-electron strongly correlated materials. For cubic NpPd<sub>3</sub> a sharp transition and change of sign in S(T) at the Néel temperature indicate a first-order nature of the magnetic transition, probably accompanied by a large change in the Fermi surface topology. We have also estimated the power factor (S<sup>2</sup>/ρ) of these materials.

## Actinides and Rare Earths

### Room 123 - Session AC+MI-ThA

#### Forensics, Disposal and Pu

**Moderators:** Itzhak Halevy, Ben Gurion Uni. Be'er Sheva, Alison Pugmire, LANL, Paul Roussel, AWE

2:15pm **AC+MI-ThA-1 A New Approach for Nuclear Forensics Investigations of Uranium Dioxide : Application of Laboratory Based Photoelectron Spectroscopy with Hard and Soft X-ray Sources, Stuart Dunn, P. Roussel, AWE, UK; A. Wood, B. Spencer, R. Harrison, University of Manchester, UK; P. Kaye, M. Higginson, AWE, UK; W. Flavell, University of Manchester, UK**

**INVITED**

Nuclear forensic investigations rely on the analysis of the chemical and physical properties to determine the provenance of nuclear materials, found out of regulatory control. X-ray photoelectron spectroscopy (XPS) has been shown to be a powerful tool in supporting material assessment by analysis of the top few nanometres of the surface. With the onset of laboratory based hard x-ray photoelectron spectroscopy (HAXPES) instrumentation, this provides the opportunity to probe deeper into the bulk. Furthermore, HAXPES spectra of high Z elements will have multiple core level peaks occurring over a range of different depths and analysis of these can offer a unique non-destructive depth profile. The work presented in this study demonstrates the utility of a combined XPS and HAXPES analysis to isolate forensic signatures on the surface and into the bulk of uranium dioxide. Survey quantification shows the changing stoichiometry, utilising a 9.25 KeV excitation range of HAXPES, from different average depths within the sample matrix. Peak fitting of high-resolution spectra allows identification of oxidation states as well inspection of secondary features, which provide insight into the material characteristics. Combined with XPS analysis, this shows different chemical and elemental states at the surface into the bulk sample, highlighting the usefulness of this approach. QUASES-Tougaard analysis was performed to determine the in-depth distribution of atoms, developing a consistent model to describe the surface overlayer, correlated to the chemical and stoichiometric differences over the excitation range. Finally, the MNN X-ray excited Auger electron spectra are acquired from uranium dioxides for the first time for use in the application of a Wagner or chemical state plot. This study is the first in a series of analysis campaigns on uranium bearing materials.

2:45pm **AC+MI-ThA-3 Making Use of X-ray Emission Signatures in the Scanning Electron Microscope to understand f-Element Speciation and Phase, Mark Croce, Los Alamos National Laboratory**

**INVITED**

While X-ray absorption spectroscopy is exquisitely sensitive to signatures of chemical speciation and phase, what if similar information could be obtained from the scanning electron microscope? Scanning electron microscopes have become more than imaging tools – they are accessible microanalysis platforms with nanoscale spatial resolution and are compatible with a wide variety of samples including those not suitable for X-ray absorption spectroscopy. Although the physics relating the chemical and physical state of an atom to X-ray emission is more complex than for X-ray absorption, there are still distinct signatures present in the X-ray emission spectra. The twofold challenge is to measure them and interpret them. Recent development in low-temperature microcalorimeter spectrometers has made it possible to simultaneously achieve the energy resolution and detection efficiency needed to observe this fine structure in X-ray emission resulting from the interaction of the microscope's electron beam with a sample. In parallel, extending molecular and atomic theory to interpret X-ray emission spectra is beginning to allow use of this capability as a research tool to determine chemical speciation and phase for f-elements including cerium, uranium, and plutonium even in non-ideal samples. We present progress towards developing what we call "Hyperspectral X-ray Imaging" using a large-array microcalorimeter X-ray spectrometer with <10 eV FWHM energy resolution at 3 keV coupled to a commercial scanning electron microscope, recent results on lanthanide and actinide samples, and future applications of the method to support f-element science.

LA-UR-24-21795

3:15pm **AC+MI-ThA-5 Automated Particle Analysis of Actinide-Bearing Nuclear Wastes, Edgar Buck, Pacific Northwest National Laboratory**  
Automated particle analysis (APA) is performed on the Scanning Electron Microscope/X-Ray Energy Dispersive Spectroscopy (SEM-EDS) and enables the characterization of morphology and composition of particles. This

method allows hundreds to thousands of particles to be examined and reduces operator bias. We have applied APA methods to radioactive Hanford tank waste materials containing rare earth elements, uranium, and plutonium. The challenge for APA with highly heterogeneous materials is the variability in particle size. An important component of the APA is the preparation of the samples for analysis and the segmentation routines used to locate particles of interest. Biased results can be generated during the deposition of particles with larger particles tending to fall out more quickly than smaller particles, and therefore can become concentrated at the center of the sample stub, where the material is directly pipetted. It is important to be aware of the factors controlling the deposition of the particles and analyze the entire SEM stub to obtain representative data. Image segmentation routines have to be calibrated to prevent missing particles and for obtaining accurate morphological data. In this presentation, we will describe the efforts to characterize and classify the actinide-rich wastes.

3:30pm **AC+MI-ThA-6 Development of X-Ray Spectromicroscopy Techniques for Nuclear Safeguards and Nuclear Forensics, David Shuh, A. Ditter, N. Cicchetti, O. Gunther, LBNL; J. Brackbill, UC Berkeley/LBNL; R. Lim, A. Baker, S. Donald, B. Chung, LLNL; R. Coles, BNL; A. Duffin, J. Ward, M. Miller, PNNL**

The on-going development of improved characterization methods and signatures is crucial to ensure that nuclear safeguards and forensics activities remain effective. For these purposes, the development of X-ray techniques is particularly useful because of their elemental specificity and non-destructive nature that could enable a first-in capability. Tunable synchrotron radiation X-ray approaches provide a means to extend the scope of safeguards and forensics investigations in elemental, chemical, and structural analysis which can be done in imaging modes that in some cases, reaches to the nanoscale. The ability to use tunable, focused X-ray beams makes synchrotron radiation sources a potentially disruptive tool for addition into the array of characterization techniques currently employed, particularly for the investigation of particles or areas of interest in smaller specimens possessing bulk-like characteristics. However, the use of synchrotron radiation methods also presents some unique challenges for the implementation of safeguards and forensic efforts at the synchrotron radiation facility sites (ALS, APS, NSLS-2, and SSRL). Synchrotron radiation-based safeguards and forensics studies over the past several years conducted at nearly all of the U.S. Dept. of Energy synchrotron radiation user facilities throughout the X-ray spectrum have furthered this case, as well as clearly identifying areas that require improvement. At the same time, there have been significant performance improvements in fixed-energy laboratory-based X-ray instrumentation suitable for contemporary, spatially-resolved safeguards and forensics (primarily XRF) studies. Additionally, there have been continued efforts and strides made towards the realization of true laboratory-based X-ray light sources that could provide competitive X-ray flux and tunability, albeit in the future, that might provide the best combination of performance and characteristics necessary for safeguards and forensics characterization activities. A current assessment of the relative strengths and drawbacks of the respective X-ray approaches, as well as a performance comparison will be presented, leading into an overall the future outlook in terms of safeguards and forensics.

3:45pm **AC+MI-ThA-7 Site-Specific and Spatially Resolved Morphological and Chemical Analysis of Plutonium and Uranium Materials, Brandon Chung, A. Baker, S. Donald, T. Li, R. Lim, U. Mehta, D. Rosas, D. Servando-Williams, N. Cicchetti, Lawrence Livermore National Laboratory; A. Ditter, O. Gunther, D. Shuh, Lawrence Berkeley National Laboratory**

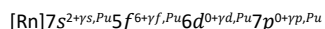
Nuclear forensics requires accurate identification of distinguishing material characteristics to delineate the material's origin-to-interdiction information. Morphological and chemical variation in nuclear materials over large scales of observation can provide valuable information that can assist interpretation of the material's varying provenance, process, and pathways. We will describe our efforts to strengthen operational and scientific methodologies to employ the focused ion beam-scanning electron microscopy (FIB-SEM) on uranium (U) and plutonium (Pu) materials for internal morphological analysis including site-specific 3D microscopy and spatially resolved characterizations of material features using transmission electron microscopy (TEM) and X-ray synchrotron spectromicroscopy. Both U and Pu materials show variations in the internal chemical composition and morphology from their production processes and storage environments. This information is of potential use in discriminating material signals to identify the origin and history of interdicted nuclear materials.



# Thursday Afternoon, November 7, 2024

## 4:00pm AC+MI-ThA-8 An Entropic Approach to Estimating Orbital Occupancies in Plutonium, *Miles Beaux*, Los Alamos National Laboratory

Janoschek, et al. described the ground state of plutonium (Pu) as being “governed by valence fluctuations, that is, a quantum mechanical superposition of localized and itinerant electronic configurations.” [*Science Advances*, 1, 6 (2015)]. By representing this ground state generally as



where  $\gamma_{s, \text{Pu}}$ ,  $\gamma_{f, \text{Pu}}$ ,  $\gamma_{d, \text{Pu}}$ , and  $\gamma_{p, \text{Pu}}$  represent potentially non-integer deviations from the integer occupancies of their respective orbitals, a combinatorial approach can be applied to the allowable permutations of quantum electronic configurations as a means of describing the electron degrees of freedom. This approach enables a classical statistical mechanics methodology to be applied to the discrete quantum states for conceptualizing and investigating the multiconfigurational ground state of Pu. Specifically, an over-approximation (with Hund’s rule relaxed) and an under-approximation (with Hund’s rule enforced) of electronic structure entropy has been established for varying ranges of potentially near energy degenerate occupancy configurations for plutonium. This bracketing of electronic structure entropy is compared with the known molar entropy of Pu to narrow down the set of possible localized and itinerant electronic configurations that can reasonably contribute to the quantum mechanical superposition of Pu’s multiconfigurational ground state, as well as to estimate the non-integer orbital occupancies of its 7s-, 5f-, 6d- and 7p-orbitals.

LA-UR-24-22282

## 4:15pm AC+MI-ThA-9 The Problem with the Second Derivative Method in EELS\*, *JG Tobin*, University of Wisconsin-Oshkosh

The second derivative mode of peak analysis in electron energy loss spectroscopy (EELS) in a Transmission Electron Microscope (TEM) has been quantitatively evaluated in terms of the accuracy of the method.\*This includes a demonstration of the importance of the second derivative peak width, the second order dependency of the accuracy upon that peak width and effect of high frequency noise in the spectra. It was found that, while EELS does converge to an X-ray Absorption Spectroscopy (XAS)-like limit (electron dipole transition) at high energies, there are significant issues with the 2<sup>nd</sup> Derivative Model.

1. There is no fixed relationship between non-derivative peak intensities and 2<sup>nd</sup> derivative peak intensities. Changing peak-shapes changes the ratio.
2. Assuming that peak-shapes remain constant, which may not be justified, there is a second order dependence of the ratio upon the peak width of the 2<sup>nd</sup> Derivative peak.
3. The second order dependence upon the peak width manifests itself in two very distinct ways: with random errors and systematic errors.
  1. The random error from high frequency noise places a limit on the number of significant digits in the BR result.
  2. The systematic error has shown up in the BR predictions and 5f population estimates (n) for the localized systems Pu, PO<sub>2</sub> and UO<sub>2</sub>.

The 2<sup>nd</sup> Derivative Mode in EELS should be used with great caution in quantitative BR analyses of 5f populations.

\*J. G. Tobin, "A quantitative evaluation of the 2nd derivative mode in electron energy loss spectroscopy," *J. Electron Spectroscopy Rel. Phen.* 268, 147387 (2023), <https://doi.org/10.1016/j.elspec.2023.147387>

## Actinides and Rare Earths

### Room Central Hall - Session AC-ThP

#### Actinides and Rare Earths Poster Session

**AC-ThP-2 Nuclear Forensics, Fission Track Analysis, Star Segmentation and Classification Using Deep Learning**, N. Elgad, R. Babayew, Y. Yehuda-Zada, Ben Gurion Uni., Israel; J. Lorincik, Research Centre Řež, Czechia; M. Last, I. Orion, G. Katarivas-Levy, Ben Gurion Uni., Israel; A. Weiss, Bar Ilan University, Israel; **Itzhak Halevy**, Ben Gurion Uni., Israel

A novel approach for identifying star shapes in microscopic images via deep learning segmentation and classification.

Semi-automated data tagging: Introducing a new method for labeling data.

U-Net FCN model: Designed for segmenting various star-like shapes in single or multi-class scenarios.

Identifying shapes under a microscope involves separating the sampling paper into ~10,000 images, akin to finding a needle in a haystack due to its grueling nature and human eye limitations.

Star identification has evolved from manual eye scans to recent advancements in automatic

image processing tools.

This work employs a deep learning model, specifically the U-Net network, for segmentation and classification, integrating a 5-fold cross-validation analysis.

Work Content:

1. A New image star database was created.
2. Characterization of star types, model architecture, and optimization.
3. Training for single and multi-class datasets.
4. Automation of segmentation for batches of images.
5. Research on optimizing frequency, epochs, and threshold settings,
6. collaborating on simulated star classification.

Model achieved 92.04% accuracy for small single-class stars (<60 $\mu$ m), with 0.84 ROC area.

Segmentation of dual-class stars reached 86.3% validation accuracy.

Identification of simulated stars with varying leaf counts achieved 82.63% accuracy, while a computational model for higher magnitude stars achieved 0.90 ROC area.

**AC-ThP-3 Tracking the Impact of Varied Oxygen Partial Pressure during PLD Growth on the Magnetic Response of Metastable Orthoferrite LuFeO<sub>3</sub>**, **Washat Ware**, M. Frye, M. Mourigal, L. Garten, Georgia Institute of Technology, USA

While the orthorhombic phase of LuFeO<sub>3</sub> (o-LFO) has attracted attention as a potential defect-induced room temperature multiferroic<sup>1</sup>, stabilizing this metastable phase while maintaining the correct defect concentrations remains a challenge. The antiferromagnetic behavior in o-LFO is thought to stem from a weak canted moment that is perpendicular to the c-axis, while ferroelectricity is attributed to anti-site defects.<sup>1,2</sup> Given the sensitivity of this material to disorder and oxygen vacancies, it is critical to understand how processing affects the magnetic and ferroelectric phase transitions of this orthoferrite. Determining the magnetic phase transition temperatures and potential for ferroic coupling within o-LFO is the first step toward reaching the full potential of this material for magnetoelectric applications.

In this work, we characterize the impact of processing on the magnetic response of o-LuFeO<sub>3</sub> grown by pulsed laser deposition (PLD). A stoichiometric LuFeO<sub>3</sub> target was used to deposit thin films onto (100) SrTiO<sub>3</sub> substrates while varying either the oxygen partial pressure (p<sub>O<sub>2</sub></sub>), laser fluence, growth temperature, or growth rate. X-Ray diffraction (XRD) indicates that the metastable orthoferrite phase is stabilized with a solely (001) orientation under all conditions. Varying the oxygen partial pressure (p<sub>O<sub>2</sub></sub>) from 0.05 mbar to 0.2 mbar, leads to a broadening of the (001) family of peaks of the o-LuFeO<sub>3</sub>, which could indicate a decrease in crystallite size, variation in orientation, or microstrain at the microscopic level. Varying laser fluences from 2 J/cm<sup>2</sup> - 2.2 J/cm<sup>2</sup> show a similar pattern of broadening but the effect is not as prominent. High temperature, vibrating sample magnetometry (VSM) is used to track the change in transition temperature under field cooling (FC) and zero field cooling (ZFC). Under FC and ZFC in the narrow field range, a phase transition is seen around 50 K and 270 K,

and a clear magnetic hysteresis is present for all samples. Building the understanding of the magnetic phase transition in orthoferrite, LuFeO<sub>3</sub> is the first step towards developing room temperature magnetoelectric coupling devices.

1. Choo, E., Klyukin, K., Su, T. Kaczmarek, A., Ross, C. "Composition-Dependent Ferroelectricity of LuFeO<sub>3</sub> Orthoferrite Thin Films," Adv. Electron. Mater. 2300059(9), 1-8 (2023).
2. Chowdhury, U. et al. "Origin of Ferroelectricity in orthorhombic LuFeO<sub>3</sub>," Phys. Rev. B. 100 (11), 1-11 (2019).

**AC-ThP-4 Electronic Structure of a Nodal Line Semimetal Candidate, Iftakhar Bin Elius**, University of Central Florida; S. Regmi, Idaho National Laboratory; A. Sakhya, University of Central Florida; V. Buturlim, Idaho National Laboratory; M. Sprague, M. Mondal, N. Valadez, University of Central Florida; T. Romanova, Polish Academy of Sciences, Poland; A. Kumay, University of Central Florida; A. Ptok, Polish Academy of Sciences, Poland; K. Gofryk, Idaho National Laboratory; D. Kaczorowski, Polish Academy of Sciences, Poland; M. Neupane, University of Central Florida

LnSbTe (Ln= lanthanides) compounds isostructural to well-known ZrSiS family of nodal line semimetals offer a rich platform for studying topological features as well as interaction of topology, magnetism, and electronic correlation owing to the presence of 4f electrons. We performed systematic magnetic field induced thermal transport, temperature dependent magnetic susceptibility and field dependent magnetization studies of rare-earth based ternary semimetals of this series at low temperature. To investigate the electronic structure of the materials, angle resolved photoemission spectroscopy (ARPES) and first principles-based calculations were performed. Multiple nodal lines along  $\Gamma$ -X and  $\Gamma$ -M high symmetry directions were observed in photon energy dependent ARPES measurements. Our investigation indicates that this system can provide a rich platform to study the interplay of magnetism, topology and correlation.

**AC-ThP-5 Grain Boundary and Heterointerface Structures and Defects in Pu Oxides: Classical Molecular Statics Study to Inform Further Ab Initio Investigation**, **Larissa Woryk**, R. Atta-Fynn, A. Kohnert, S. Hernandez, Los Alamos National Laboratory

Plutonium metal forms a passivated oxide layer upon exposure to air, with varying stoichiometry depending on oxygen conditions. At lower temperatures, interfaces in oxides can facilitate corrosion via fast-transport pathways. This can result in further growth of the oxide layers, or of corrosion via other species, such as hydriding from the absorption and transport of hydrogen throughout the material. Any of these forms of corrosion can have implications on the stability and longevity of material in storage. Structural, defect, and transport properties can vary across different grain boundaries and heterointerface orientations. This study presents structures and associated energies of selected Pu<sub>2</sub>O<sub>3</sub>-PuO<sub>2</sub> interfaces and selected grain boundaries, calculated with molecular statics, along with associated defect structures and formation energies. Comparisons of interfacial energies can suggest which interfaces might be more prevalent in these materials, which could then play a larger role in influencing material properties and behavior. Comparisons of defect energies, both across different interfaces and between interfaces and in bulk, can suggest influence of interfaces in corrosion and in transport phenomena more broadly.

The Cooper-Rushton-Grimes interatomic potential will be utilized for the molecular statics calculations as it has demonstrated comparable values to experimental lattice and elastic constants, and thermal properties [1]. Where applicable, the modification to this potential to include Pu<sup>3+</sup> is also included, as developed by Takoukam-Takoundjou, *et al* [2].

[1] M W D Cooper *et al* 2014 *J. Phys.: Condens. Matter* **26** 105401.

[2] C Takoukam-Takoundjou *et al* 2020 *J. Phys.: Condens. Matter* **32** 505702.

**AC-ThP-6 Exploring the Combined Influence of Alpha Irradiation, Dissolved Hydrogen, and Palladium Addition on UO<sub>2</sub> Corrosion Using a Microfluidic Electrochemical Cell**, **Jennifer Yao**, J. Heo, B. McNamara, E. Ilton, E. Buck, PNNL

Understanding the influence of alpha irradiation and dissolved hydrogen on the corrosion behavior of uranium dioxide (UO<sub>2</sub>) is essential for evaluating the long-term impacts on storage environments.[1] Traditional experiments involving bulk SNF are typically costly due to stringent requirements for radiation shielding. To address these challenges, we have developed a novel particle-attached microfluidic electrochemical cell (PAMEC). This innovative microfluidic technique enables the multimodal analysis of UO<sub>2</sub> corrosion

# Thursday Evening, November 7, 2024

under simulated SNF storage conditions using minimal material quantities, significantly reducing both costs and risks of hazardous exposure.[2, 3]

Recently, we have incorporated palladium—a noble metal commonly found in irradiated nuclear fuel—into the  $\text{UO}_2$  working electrode. This modification allows us to investigate how noble metals influence  $\text{UO}_2$  degradation behavior in the presence of dissolved  $\text{H}_2$  and alpha irradiation. In addition to utilizing electrochemical measurements such as open circuit potential, for qualitative insights into the degradation of the  $\text{UO}_2$  matrix, PAMEC's unique design supports in situ chemical imaging of the  $\text{UO}_2$  surface. In this study we employ in situ imaging of the PAMEC working electrode using scanning electron microscopy (SEM) combined with energy-dispersive X-ray spectroscopy (EDS). This integration of techniques offers a comprehensive view that enhances our understanding of the  $\text{UO}_2$  corrosion mechanism. The potential applications of this technology are extensive, providing a safer and more effective alternative for conducting corrosion studies on materials that pose high exposure risks or are difficult to access due to their rarity.

References:

1. *Long-term storage of spent nuclear fuel*. Nature Materials, 2015. **14**(3): p. 252-257.
2. *A microfluidic electrochemical cell for studying the corrosion of uranium dioxide ( $\text{UO}_2$ )*. RSC Adv, 2022. **12**(30): p. 19350-19358.
3. *Advancing radioactive material research method: the development of a novel in situ particle-attached microfluidic electrochemical cell*. Frontiers in Nuclear Engineering, 2023. **2**.

## Actinides and Rare Earths

### Room 123 - Session AC+MI-FrM

#### Actinide and Rare Earth Chemistry and Physics

**Moderators:** Edgar Buck, PNNL, Krzysztof Gofryk, Idaho National Laboratory, Gertrud Zwignagl, Technical University Braunschweig

8:15am **AC+MI-FrM-1 Structure, Stability, and Chemistry of Actinide Nanoparticles**, Ping Yang, G. Wang, E. Batista, Los Alamos National Laboratory **INVITED**

Nanoscale materials bearing heavy elements have a wide range of applications from the nuclear fuel cycle to environment and health. Nanocrystals (NCs) with size and shape dependent properties are a thriving research field and remarkable progress has been made in the controlled synthesis and characterization of NCs composed of stable elements in the past three decades. In this context, interfacial chemistry of nano-sized materials is critical for controlling the morphology that drives their unique associated chemical and physical properties. The understanding of NCs containing f-elements is comparatively limited due to difficulties in handling them both experimentally and theoretically. In this talk, I will share some recent progress in understanding the interplay between surface energy, surfactant ligands, and the chemistry in determining the morphology of 5f-element nanoparticles. Quantum simulations provide a molecular-level picture of the relevant driving forces and dynamic properties. To push for larger lengthscale, we recently developed the density functional theory tight-binding (DFTB) parameters for actinide systems, that enabled the microsecond quantum MD simulations of actinide nanoparticle systems.

[1] G Wang, ER Batista, P Yang, *Phys Chem Chem Phys* **2018**, *20*, 17563

[2] G Wang, ER Batista, P Yang, *J. Phys Chem C*, **2019**, *123*, 30245

[3] RK Carlson, MJ Cawkwell, ER Batista, P Yang, *J. Chem. Theor. Compt* **2020**, *16*, 3073

[4] NF Aguirre, J Jung, P Yang, *Phys Chem Chem Phys* **2020**, *22*, 18614

[5] G Wang, ER Batista, P Yang, *Appl Sci* **2020**, *10*, 4655

[6] D G Gonzalez, G Wang, ER Batista, P Yang, *Inorg Chem* **2023**, *in press*

8:45am **AC+MI-FrM-3 The Use of Ligand Modified Electrodes as Electrocatalysts for Actinide Redox Chemistry**, Christopher Dares, Florida International University; T. Grimes, Idaho National Laboratory; J. McLachlan, University of California at Berkeley; X. Hou, University of Utah; A. Ruiz Reyes, Florida International University **INVITED**

The lanthanides are most stable in the trivalent oxidation state, and with few exceptions, are difficult to generate in higher or lower oxidation states. In contrast the early actinides are redox active and can be generated and studied in a variety of oxidation states ranging from +7 to +2. This variety can complicate separations processes since oxidation state and can have a profound influence on ligand binding and solvent extraction. Separations schemes can also exploit the differences in binding preferences in different oxidation states to make selective extraction more efficient. In an aqueous acidic environment, the Am(IV/III) couple is at 2.6 V vs. the standard hydrogen electrode (SHE). This is nearly at the limit of what is possible in an aqueous solution where the 1-electron oxidation of water to hydroxyl radical is only about 0.3 V more positive. The subsequent potentials to generate penta- and hexavalent americium are lower though the high Am(IV/III) couple renders Am effectively redox-inert. Ligand coordination can be used to reduce the Am(IV/III) couple and/or facilitate the proton-coupled electron transfer (required to make the americium cation). These can be organic ligands including N-donors or inorganic ligands such as lacunary polyoxometalates. Ligands anchored to metal oxide electrodes serve as good electrocatalysts to generate Am(V) or Am(VI) and operate at potentials as low as 1.6 V vs. SCE (nearly 1 V below the Am(IV/III) couple). Ligands are attached to the surface using either organic functional groups like phosphonic acids, or, through a combination of attractive interactions including hydrogen-bonding. They form well-packed monolayers on mesoporous thin layers of conductive oxides. The development of these ligand modified electrodes (LMEs) will be introduced along with characterization of their ability to adjust actinide oxidation states.

9:15am **AC+MI-FrM-5 Observation of Flat Bands in Rare-Earth Based Kagome Metals**, Madhab Neupane, University of Central Florida **INVITED**  
Quantum materials with kagome lattice – comprised of corner-sharing triangles forming a hexagon in the crystal structure – have been studied as the potential playgrounds for exploring the interplay among parameters

such as geometry, topology, electronic correlations, magnetic, and charge density orders. Recent report on a family of kagome metals of the form  $\text{ReTi}_3\text{Bi}_4$  (Re = rare-earth) has generated interest due to the combination of highly anisotropic magnetism and a rich electronic structure. We use angle-resolved photoemission spectroscopy measurements in combination with density functional theory calculations to investigate the electronic structure of newly discovered kagome metals  $\text{ReTi}_3\text{Bi}_4$ . Our results reveal multiple van Hove singularities (VHSs), some of which are in the vicinity of the Fermi level. We clearly observe multiple flat bands, which originate from the destructive interference of wave functions within the Ti kagome motif. These flat bands and VHSs originate from Ti d-orbitals and are very responsive to the polarization of the incident beam. These results demonstrate that of Ti based kagome materials system is an excellent material platform for studying kagome induced flat band physics and its connection with magnetism.

9:45am **AC+MI-FrM-7 Kinetics and Mechanism of Plutonium Oxycarbide Formation**, Paul Rousset, AWE plc, UK

Plutonium is both electropositive and highly reactive, such that an oxide film of varying thickness is always present on metal samples. It is of interest from a safety point of view (reduced handling/processing) to investigate methods that either prevent or slow down the rate of corrosion reaction of the metal. Plutonium oxycarbide,  $\text{PuC}_{1-x}\text{O}_x$ , surface films on plutonium metal have shown the ability to slow the rate of oxidation [1]. Favart *et al.* have reported the rate of plutonium oxycarbide formation at 350 °C [2] as measured using X-ray Diffraction. In the theoretical study reported by Qiu *et al.* the authors proposed four different mechanisms for the formation of plutonium oxycarbide [3]. Two of the proposed mechanisms involved the reaction of a gas with plutonium sesquioxide,  $\text{Pu}_2\text{O}_3$ , and the other two involved a solid state reaction of this oxide to form plutonium oxycarbide. Using a combination X-ray Photoelectron Spectroscopy, Secondary Ion Mass Spectrometry and X-ray Diffraction the kinetics and mechanism of plutonium oxycarbide formation have been investigated and will be presented.

[1] Retardation of plutonium oxidation by a PuO surface film, D. T. Larson, D. L. Cash, *J. Vac. Sci. Technol.* **9**, 800 (1972).

[2] Characterization of PuO/PuCO phase and its influence on the oxidation kinetics of d-plutonium, N. Favart, B. Ravat, L. Jolly, B. Oudot, L. Berlu, F. Delaunay, I. Popa, S. Chevalier, *Oxid. Met.*, **96**, 271 (2021)

[3] Thermodynamical stability of plutonium monoxide with carbon substitution, R. Qiu, X. Wang, Y. Zhang, B. Ao, K. Liu, *J. Phys. Chem. C* **122**, 22821 (2018).

10:00am **AC+MI-FrM-8 Layered f-Metal Zintl Phases -  $\text{EuZn}_2\text{P}_2$  and  $\text{UCu}_2\text{P}_2$** , LADISLAV HAVELA, Charles University, Czech Republic; V. Buturlim, Idaho National Laboratory; O. Koloskova, Charles University, Prague, Czechia; D. Legut, J. Prchal, Charles University, Czech Republic; J. Kolorenc, J. Kastil, M. Misek, Institute of Physics CAS, Prague, Czechia

Zintl phases consisting of an electropositive element, cation, and covalently bonded polyanion, offer a large variability of electronic structure, bridging the gap between semiconducting and metallic behavior and offering interesting functionalities. In case of magnetic cation, properties can be further tuned by magnetic fields. Here we compare compounds based on lanthanide (Eu) and actinide (U) cations. We selected layered compounds, crystallizing in the trigonal structure  $\text{CaAl}_2\text{Si}_2$ , which exhibit pronounced magnetic anisotropy.  $\text{EuZn}_2\text{P}_2$  is a narrow band-gap semiconductor. Antiferromagnetic ordering of  $\text{Eu}^{2+}$  moments sets in at  $T_N = 23$  K. Rapid increase of  $T_N$  with applied pressure, which reaches 43 K at  $p = 9.5$  GPa, can be associated with reduction of the band gap, indicated by transport properties as well as by ab-initio calculations. Ferromagnetic alignment of Eu moments, achieved in fields of several Tesla, can reduce electrical resistivity by several orders of magnitude, which is classified as Colossal Magnetoresistance Effect. At  $p = 18$  GPa (still within the same structure type),  $\text{EuZn}_2\text{P}_2$  becomes semi-metallic. The compression by hydrostatic pressure is anisotropic, with soft c-axis direction.  $\text{UCu}_2\text{P}_2$  with a smaller unit-cell volume is semi-metallic (and probably half-metallic) at ambient conditions. Also here the magnetic order (ferromagnetic) is supported by applied pressure, reaching 290 K at 6 GPa. The situation of 5f states is dramatically different comparing with the 4f states in the Eu counterpart. The indications given by large spontaneous magnetostriction, softer a-axis direction (nearest U-U links), or extremely strong uniaxial magnetocrystalline anisotropy point to an involvement of the 5f states in bonding, i.e. delocalization, although they do not contribute to the Fermi level, located in a pseudo-gap. Tuning by composition changes is not

# Friday Morning, November 8, 2024

straightforward for single crystals grown by Chemical Vapor Transport method, nevertheless certain routes have been attempted with a positive outcome and properties of doped  $\text{UCu}_2\text{P}_2$  will be discussed.

10:30am **AC+MI-FrM-10 Experimental Electronic Structure Measurements of Actinide-Containing Samples Using Scanning Tunneling Spectroscopy**, Benjamin Heiner, M. Beaux, Los Alamos National Laboratory

The many difficulties performing experiments on plutonium-containing samples makes the prospect of studying them using computational methods enticing. The lag in collection of experimental data using modern techniques, especially related to electronic structure, has made validating computational methods challenging. With the establishment of a scanning tunneling microscope at Los Alamos National Laboratory with the capacity to study plutonium and other radioactive samples, the ability to probe electronic structure seamlessly across the Fermi energy is now possible. In a first of its kind experiment, scanning tunneling spectroscopy data on plutonium-containing samples, especially gallium-stabilized  $\delta$ -phase plutonium, has been collected. The spectra reveal a surface with semimetal characteristics instead of a computationally predicted semiconductor band gap.

LA-UR-24-24274

10:45am **AC+MI-FrM-11 Unconventional Superconductivity in  $\text{UBe}_{13}$  - Investigation via Variation of Impurity Level - and Comparison to the Conventional Superconductor  $\text{LuBe}_{13}$** , Greg Stewart, J. Kim, University of Florida

We have prepared and characterized down to  $T=0.40$  K three arc-melted samples each of  $\text{MBe}_{13}$ ,  $M = \text{Lu}, \text{U}$ , using threedifferent purities (99.999%, 99.96%, and 99.8%) of Be but with the same high purity  $M$  ( $\text{Lu}$  or  $\text{U}$ ) for all three. The measurements down to 0.40 K allow the detection of the maximum in the specific heat in all three  $\text{LuBe}_{13}$  samples. The resulting superconducting properties **strongly** depend on impurity level in  $\text{UBe}_{13}$  (40% decrease in  $\Delta C/T_c$ , 15% decrease in  $T_c$ mid) while the three  $\text{LuBe}_{13}$  samples exhibit significantly smaller changes (10% and 5% respectively) with purity. The comparison of properties at the first two levels of purity (99.999% vs 99.96%) is even more disparate: 12% decrease in  $T_c$ mid in  $\text{UBe}_{13}$  vs no change in  $\text{LuBe}_{13}$ . These results are consistent with previous results that argue for unconventional superconductivity in  $\text{UBe}_{13}$ , and are consistent with assignment of  $\text{LuBe}_{13}$  as a conventional, BCS superconductor. As will be discussed in more detail, this example of comparing superconducting properties vs controlled gradations in impurity levels with two compositionally and structurally “matched” superconducting compounds (one conventional and one of to-be-determined coupling behavior) offers a new method - versus the already existing ones - for determining unconventional superconducting behavior.

11:00am **AC+MI-FrM-12 Strong Magnetoelastic Interactions in HoSb Probed by High-Resolution Dilatometry and X-Ray Diffraction**, Volodymyr Buturlim, Glenn T. Seaborg Institute, Idaho National Laboratory; N. Poudel, Idaho National Laboratory; D. Kaczorowski, Polish Academy of Sciences, Poland; M. Jaime, Physikalisch Technische Bundesanstalt, Germany; Z. Islam, Argonne National Laboratory; K. Gofryk, Center for Quantum Actinide Science and Technology, Idaho National Laboratory

Rare-earth (RE) mononictides, which crystallize in a cubic structure similar to NaCl have drawn considerable interest due to their diverse transport, magnetic, and structural properties. The non-magnetic compounds are known for the transition from topological to trivial electronic states (e.g.  $\text{LaPn}$  where  $\text{Pn} = \text{Bi}$  and  $\text{As}$  [1]). Magnetism of the compounds with long-range order brings complexity to their topological properties. However, the topological nature of these materials undergoes intense debates and investigation. HoSb is a topologically trivial semimetal, which orders antiferromagnetically below  $T_N = 5.7$  K [2]. Application of magnetic field leads to the change of its magnetic structure from MnO-type antiferromagnetic (AFM) arrangement to HoP-type arrangement, then to ferromagnetic (FM) arrangement. There are also reports which suggest a transition to tetragonal structure taking place at  $T_N$  [3]. The variety of the low-temperature phenomena makes HoSb a good platform to investigate the role of magnetic ordering and the strength of spin-phonon coupling on the crystal structure of this system. We will present the results of low-temperature high-resolution dilatometry as well as X-ray diffraction studies performed at static and pulsed magnetic fields. Heat capacity studies and the presence of latent heat agree with the structural distortion that occurs at  $T_N$ . The lowering of the symmetry is further supported by detailed low-temperature X-ray diffraction measurements under magnetic fields. Strong spin-lattice coupling in HoSb results in giant magnetostriction of the order of 1500 ppm. Furthermore, our detailed dilatometry studies allow us to

construct a magnetic phase diagram of HoSb. We will discuss the implications of these results in the context of the strong magnetoelastic properties in HoSb and other rare-earth mononictides.

[1] H. Y. Yang et al., Phys. Rev. B **98**, 045136 (2018).

[2] M. M. Hosen et al., Sci. Reports 2020 101 **10**, 1 (2020).

[3] F. Lévy, Phys. Kondens. Mater. **10**, 85 (1969).

KG acknowledges the support from the Division of Materials Science and Engineering, Office of Basic Energy Sciences, Office of Science of the U. S. Department of Energy (U.S. DOE). VB acknowledges the support from the Idaho National Laboratory's Laboratory Directed Research and Development (LDRD) program under DOE Idaho Operations Office Contract DE-AC07-05ID14517.

11:15am **AC+MI-FrM-13 Electronic Structure in a Rare-Earth-Based Intermetallic System  $\text{TbNi}_3\text{Ga}_9$** , Sabin Regmi, V. Buturlim, Idaho National Laboratory; B. Rai, Savannah River National Laboratory; T. Durakiewicz, K. Gofryk, Idaho National Laboratory

Rare-earth-based intermetallics provide flexibility to study the electronic, magnetic, superconducting, and topological properties by tuning the crystal structure, composition, and spin-orbit coupling. Recently,  $\text{RNi}_3(\text{Ga/Al})_9$  intermetallic materials have been studied for their richness in broad range of exotic crystal, magnetic, heavy fermion, and quantum criticality behaviors. However, momentum-resolved electronic structure studies are lacking. Here, we present results of the angle-resolved photoemission spectroscopy measurements to reveal the underlying electronic structure and topology in  $\text{TbNi}_3\text{Ga}_9$ , both above and below the Néel temperature. This study will open up exciting avenues towards exploration of electronic properties in the chiral family of  $\text{RNi}_3(\text{Ga/Al})_9$  materials with wide range of intriguing properties.

11:30am **AC+MI-FrM-14 Catalytic Activities of Defected Actinide Dioxide  $\text{AnO}_2$  Surface: A First Principles Study**, Shukai Yao, G. Wang, E. Batista, P. Yang, Los Alamos National Laboratory

Actinide dioxides  $\text{AnO}_2$  play an important role as nuclear fuels in commercial nuclear reactors. Understanding the surface chemistry of  $\text{AnO}_2$  is crucial in various aspects such as safe operations, recycling, and storage of nuclear fuels. Actinide materials have shown to be highly efficient catalyst for the activation of  $\text{H}_2$ ,  $\text{CO}$ ,  $\text{NH}_3$ , etc., mainly due to valent 5f electrons of actinides characterized by strong electron correlations and various oxides states. However, experimental studies of actinide systems are limited by their high safety requirement associated with radioactivity. In this computational study, we employed first principles electronic structure calculations based on density functional theory (DFT) to reveal the catalytic behavior of  $\text{AnO}_2$  surface with O vacancies. We will show that O vacancies significantly change the electronic structure of  $\text{AnO}_2$  surfaces, and act as the active sites of small molecules adsorption. As a result, defected  $\text{AnO}_2$  surface leads to an enhanced reactivity compared to the pristine  $\text{AnO}_2$  surface.

11:45am **AC+MI-FrM-15 Thin Film Synthesis of Rare Earth and Actinide Nitrides Using Molecular Beam Epitaxy**, Keivn Vallejo, B. May, Z. Cresswell, V. Buturlim, S. Regmi, K. Gofryk, Idaho National Laboratory

Lanthanide- and actinide-based nitride compounds are an understudied group of materials compared to their oxide counterparts, which provide new avenues for nuclear reactor designs. Their 4f and 5f electron shell gives rise to a variety of interesting physics such as magnetism and unconventional superconductivity. Samarium nitride ( $\text{SmN}$ ) has been recently identified as a material where ferromagnetic order and potential p-type superconductivity coexist. Our team will present results on the growth conditions in a molecular beam epitaxy chamber of pure and doped  $\text{SmN}$  using molecular beam epitaxy, and its electronic transport properties as a function of temperature and magnetic field. CeN and UN thin films are also explored. The presence of  $\text{SmN}(111)$  peaks on (001) substrates indicates an orientation-preference for some material systems. The electrical resistivity and magnetic susceptibility studies have shown a range of magnetic behaviors, including paramagnetic and ferromagnetic. With a potential superconductive transition around  $\sim 10$  K,  $\text{SmN}$  and its doping effects on crystal structure and electronic properties are characterized.

**Bold page numbers indicate presenter**

— A —

Abbas, Ali: MI+2D+AC+TF-WeA-4, 4;  
MI+2D+AC+TF-WeM-7, 2; MI+2D+AC+TF-WeM-8, **2**  
Argyropoulos, Christos: MI+2D+AC+TF-WeA-10, 5  
Atta-Fynn, Raymond: AC-ThP-5, 10  
— B —  
Babayew, Rami: AC+MI-ThM-13, 7; AC-ThP-2, 10  
Baker, Alexander: AC+MI-ThA-6, 8; AC+MI-ThA-7, 8  
Bansil, Arun: MI+2D+AC+TF-WeA-3, 4  
Barreto, Lucas: MI+2D+AC+TF-WeM-14, **2**  
Batista, Enrique: AC+MI-FrM-1, 12; AC+MI-FrM-14, 13  
Bauer, Eric D.: AC+MI-ThM-3, 6  
Beaux, Miles: AC+MI-FrM-10, 13; AC+MI-ThA-8, **9**  
Bentmann, Hendrik: MI+2D+AC+TF-WeM-1, 1  
Bhandari, Ghadendra: MI+2D+AC+TF-WeM-4, **1**  
Bhattacharjee, Nirjhar: MI+2D+AC+TF-WeA-3, 4  
Bin Elius, Iftakhar: AC-ThP-4, **10**  
Binek, Christian: MI+2D+AC+TF-WeA-10, 5  
Borgschulte, Andreas: MI+2D+AC+TF-WeA-11, 5  
Brackbill, Joseph: AC+MI-ThA-6, 8  
Briley, Chad: MI+2D+AC+TF-WeA-10, 5  
Buck, Edgar: AC+MI-ThA-5, **8**; AC-ThP-6, 10  
Buturlim, Voldymyr: AC+MI-FrM-15, 13  
Buturlim, Volodymyr: AC+MI-FrM-12, **13**; AC+MI-FrM-13, 13; AC+MI-FrM-8, 12; AC-ThP-4, 10  
— C —

Chi, Hang: MI+2D+AC+TF-WeA-1, **4**  
Christovam, Denise S.: AC+MI-ThM-3, 6; AC+MI-ThM-7, 6  
Chung, Brandon: AC+MI-ThA-6, 8; AC+MI-ThA-7, **8**  
Cicchetti, Nic: AC+MI-ThA-6, 8  
Cicchetti, Nick: AC+MI-ThA-7, 8  
Coles, Rebecca: AC+MI-ThA-6, 8  
Cresswell, Zachery: AC+MI-FrM-15, 13  
Croce, Mark: AC+MI-ThA-3, **8**  
— D —  
Dares, Christopher: AC+MI-FrM-3, **12**  
Darwin, Emily: MI+2D+AC+TF-WeA-11, 5  
Dewasurendra, Vikum: MI+2D+AC+TF-WeM-4, 1  
Ditter, Alexander: AC+MI-ThA-6, 8; AC+MI-ThA-7, 8  
Donald, Scott: AC+MI-ThA-6, 8; AC+MI-ThA-7, 8  
Donath, Markus: MI+2D+AC+TF-WeM-13, **2**  
Dryzhakov, Bogdan: MI+2D+AC+TF-WeA-9, 5  
Dubs, Carsten: MI+2D+AC+TF-WeA-3, 4  
Duffin, Andrew: AC+MI-ThA-6, 8  
Dunn, Stuart: AC+MI-ThA-1, **8**  
Durakiewicz, Tomasz: AC+MI-FrM-13, 13  
— E —

Elfimov, Ilya: AC+MI-ThM-3, 6  
Elgad, Noam: AC+MI-ThM-13, 7; AC-ThP-2, 10  
Erickson, Tyler: MI+2D+AC+TF-WeM-7, 2  
— F —  
Feder, Rene: MI+2D+AC+TF-WeA-10, 5  
Figgemeier, Tim: MI+2D+AC+TF-WeM-1, 1  
Flavell, Wendy: AC+MI-ThA-1, 8  
Frye, Marshall: AC-ThP-3, 10  
Fujimori, Shin-ichi: AC+MI-ThM-1, **6**

— G —  
Gai, Zheng: MI+2D+AC+TF-WeM-3, 1  
Garten, Lauren: AC-ThP-3, 10  
Gayles, Jacob: MI+2D+AC+TF-WeM-15, 2  
Geldiyev, Begmuhammet: MI+2D+AC+TF-WeM-1, 1  
Gloskovskii, Andrei: AC+MI-ThM-3, 6; AC+MI-ThM-7, 6  
Gofryk, Krzysztof: AC+MI-FrM-12, 13; AC+MI-FrM-13, 13; AC+MI-FrM-15, 13; AC+MI-ThM-15, **7**; AC-ThP-4, 10  
Green, Robert: MI+2D+AC+TF-WeM-14, 2  
Gretarsson, Hlynur: AC+MI-ThM-7, 6  
Gretarsson, Hlynur: AC+MI-ThM-3, 6  
Grimes, Travis: AC+MI-FrM-3, 12  
Griveau, J-C: AC+MI-ThM-15, 7  
Grutter, Alexander: MI+2D+AC+TF-WeA-3, 4  
Gunther, Olivia: AC+MI-ThA-6, 8; AC+MI-ThA-7, 8  
— H —  
Halevy, Itzhak: AC+MI-ThM-13, **7**; AC-ThP-2, **10**  
Hall, Hannah: MI+2D+AC+TF-WeM-7, 2  
Hammer, Lutz: MI+2D+AC+TF-WeM-13, 2  
Hariki, Atsushi: AC+MI-ThM-7, 6  
Harrison, Ian: MI+2D+AC+TF-WeM-3, 1  
Harrison, Robert: AC+MI-ThA-1, 8  
HAVELA, LADISLAV: AC+MI-FrM-8, **12**  
Haverkort, Maurits W.: AC+MI-ThM-3, 6  
Heiman, Don: MI+2D+AC+TF-WeA-3, 4  
Heiner, Benjamin: AC+MI-FrM-10, **13**  
Heo, Jaeyoung: AC-ThP-6, 10  
Hernandez, Sarah: AC-ThP-5, 10  
Higginson, Matthew: AC+MI-ThA-1, 8  
Holcomb, Mikel: MI+2D+AC+TF-WeM-4, 1  
Hou, Xiangyang: AC+MI-FrM-3, 12  
Hu, Bin: MI+2D+AC+TF-WeA-9, 5  
Hug, Hans Josef: MI+2D+AC+TF-WeA-11, 5  
— I —  
Ilton, Eugene: AC-ThP-6, 10  
Ingram, David C.: MI+2D+AC+TF-WeA-4, 4  
Islam, Zahir: AC+MI-FrM-12, 13  
— J —  
Jaime, Marcelo: AC+MI-FrM-12, 13  
Jin, Rongying: MI+2D+AC+TF-WeM-3, 1  
Johnson, Matthew: MI+2D+AC+TF-WeM-4, 1  
— K —  
Kaczorowski, Dariusz: AC+MI-FrM-12, 13; AC-ThP-4, 10  
Karbasizadeh, Siavash: MI+2D+AC+TF-WeM-3, 1  
Kastil, Jiri: AC+MI-FrM-8, 12  
Katarivas-Levy, Galit: AC+MI-ThM-13, 7; AC-ThP-2, 10  
Kaye, Philip: AC+MI-ThA-1, 8  
Keimer, Bernhard: AC+MI-ThM-3, 6; AC+MI-ThM-7, 6  
Kilic, Ufuk: MI+2D+AC+TF-WeA-10, 5  
Kim, Jungsoo: AC+MI-FrM-11, 13  
KiBlinger, Tilman: MI+2D+AC+TF-WeM-13, 2  
Knafo, William: AC+MI-ThM-5, 6  
Kohnert, Aaron: AC-ThP-5, 10  
Kolorenc, Jindrich: AC+MI-FrM-8, 12  
Koloskova, Oleksandra: AC+MI-FrM-8, 12  
Kong, Deija: MI+2D+AC+TF-WeM-3, **1**  
Koroluk, Skylar: MI+2D+AC+TF-WeM-14, 2  
Krüger, Peter: MI+2D+AC+TF-WeM-13, 2  
Kumay, Arun: AC-ThP-4, 10  
Kunes, Jan: AC+MI-ThM-7, 6  
— L —  
Last, Mark: AC+MI-ThM-13, 7; AC-ThP-2, 10  
Lauter, Valeria: MI+2D+AC+TF-WeA-3, 4; MI+2D+AC+TF-WeA-9, 5  
Lefler, Benjamin: MI+2D+AC+TF-WeM-14, 2

— G —

Legut, Dominik: AC+MI-FrM-8, 12  
Li, Tian: AC+MI-ThA-7, 8  
Lidsky, David: MI+2D+AC+TF-WeA-3, 4  
Lim, Rachel: AC+MI-ThA-6, 8; AC+MI-ThA-7, 8  
Lindner, Morris: MI+2D+AC+TF-WeA-3, 4  
Longo, Filippo: MI+2D+AC+TF-WeA-11, **5**  
Loricink, Jan: AC+MI-ThM-13, 7; AC-ThP-2, 10  
Lu, Tzu-Ming: MI+2D+AC+TF-WeA-3, 4  
Luo, Bin: MI+2D+AC+TF-WeA-3, **4**  
— M —  
Marino, Andrea: AC+MI-ThM-3, 6; AC+MI-ThM-7, 6  
Matzelle, Matthew: MI+2D+AC+TF-WeA-3, 4  
May, Brelon: AC+MI-FrM-15, 13  
May, Steven: MI+2D+AC+TF-WeM-14, 2  
McEwen, K. A.: AC+MI-ThM-15, 7  
McLachlan, Jeffrey: AC+MI-FrM-3, 12  
McNamara, Bruce: AC-ThP-6, 10  
Mehta, Uday: AC+MI-ThA-7, 8  
Miller, Micah: AC+MI-ThA-6, 8  
Misek, Martin: AC+MI-FrM-8, 12  
Mock, Alyssa: MI+2D+AC+TF-WeA-10, 5  
Mondal, Mazharul Islam: AC-ThP-4, 10  
Monson, Todd C.: MI+2D+AC+TF-WeA-3, 4  
Mourigal, Martin: AC-ThP-3, 10  
Mu, Sai: MI+2D+AC+TF-WeM-3, 1  
— N —  
Narasimha, Ganesh: MI+2D+AC+TF-WeM-3, 1  
Nellis, W. J.: AC+MI-ThM-15, 7  
Neupane, Madhab: AC+MI-FrM-5, **12**; AC-ThP-4, 10  
— O —  
Orion, Itzhak: AC+MI-ThM-13, 7; AC-ThP-2, 10  
— P —  
Pantano, Gina: MI+2D+AC+TF-WeM-15, **2**  
Pearce, Charles J.: MI+2D+AC+TF-WeA-3, 4  
Peremadathil Pradeep, Reshma: MI+2D+AC+TF-WeA-11, 5  
Poudel, Narayan: AC+MI-FrM-12, 13  
Prchal, Jiri: AC+MI-FrM-8, 12  
Ptok, Andrzej: AC-ThP-4, 10  
Puggioni, Danilo: MI+2D+AC+TF-WeM-14, 2  
— R —  
Rai, Binod K.: AC+MI-FrM-13, 13  
Regmi, Paras: MI+2D+AC+TF-WeM-3, 1  
Regmi, Sabin: AC+MI-FrM-13, **13**; AC+MI-FrM-15, 13; AC-ThP-4, 10  
Reimann, Timmy: MI+2D+AC+TF-WeA-3, 4  
Reinert, Friedrich: MI+2D+AC+TF-WeM-1, 1  
Rogge, Paul: MI+2D+AC+TF-WeM-14, 2  
Romanova, Tetiana: AC-ThP-4, 10  
Rondinelli, James: MI+2D+AC+TF-WeM-14, 2  
Rosa, Priscila F. S.: AC+MI-ThM-3, 6  
Rosas, Debra: AC+MI-ThA-7, 8  
Roussel, Paul: AC+MI-FrM-7, **12**; AC+MI-ThA-1, 8  
Ruiz Reyes, Alberto: AC+MI-FrM-3, 12  
Russell, Daniel: MI+2D+AC+TF-WeM-8, 2  
— S —  
Sakhya, Anup Pradhan: AC-ThP-4, 10  
Schmidt, Heidemarie: MI+2D+AC+TF-WeA-10, 5  
Schneider, M. Alexander: MI+2D+AC+TF-WeM-13, 2  
Schöttke, Fabian: MI+2D+AC+TF-WeM-13, 2  
Schubert, Eva: MI+2D+AC+TF-WeA-10, 5  
Schubert, Mathias: MI+2D+AC+TF-WeA-10, 5  
Sekora, Derek: MI+2D+AC+TF-WeA-10, 5  
Servando-Williams, Donya: AC+MI-ThA-7, 8

— M —  
Marino, Andrea: AC+MI-ThM-3, 6; AC+MI-ThM-7, 6  
Matzelle, Matthew: MI+2D+AC+TF-WeA-3, 4  
May, Brelon: AC+MI-FrM-15, 13  
May, Steven: MI+2D+AC+TF-WeM-14, 2  
McEwen, K. A.: AC+MI-ThM-15, 7  
McLachlan, Jeffrey: AC+MI-FrM-3, 12  
McNamara, Bruce: AC-ThP-6, 10  
Mehta, Uday: AC+MI-ThA-7, 8  
Miller, Micah: AC+MI-ThA-6, 8  
Misek, Martin: AC+MI-FrM-8, 12  
Mock, Alyssa: MI+2D+AC+TF-WeA-10, 5  
Mondal, Mazharul Islam: AC-ThP-4, 10  
Monson, Todd C.: MI+2D+AC+TF-WeA-3, 4  
Mourigal, Martin: AC-ThP-3, 10  
Mu, Sai: MI+2D+AC+TF-WeM-3, 1  
— N —  
Narasimha, Ganesh: MI+2D+AC+TF-WeM-3, 1  
Nellis, W. J.: AC+MI-ThM-15, 7  
Neupane, Madhab: AC+MI-FrM-5, **12**; AC-ThP-4, 10  
— O —  
Orion, Itzhak: AC+MI-ThM-13, 7; AC-ThP-2, 10  
— P —  
Pantano, Gina: MI+2D+AC+TF-WeM-15, **2**  
Pearce, Charles J.: MI+2D+AC+TF-WeA-3, 4  
Peremadathil Pradeep, Reshma: MI+2D+AC+TF-WeA-11, 5  
Poudel, Narayan: AC+MI-FrM-12, 13  
Prchal, Jiri: AC+MI-FrM-8, 12  
Ptok, Andrzej: AC-ThP-4, 10  
Puggioni, Danilo: MI+2D+AC+TF-WeM-14, 2  
— R —  
Rai, Binod K.: AC+MI-FrM-13, 13  
Regmi, Paras: MI+2D+AC+TF-WeM-3, 1  
Regmi, Sabin: AC+MI-FrM-13, **13**; AC+MI-FrM-15, 13; AC-ThP-4, 10  
Reimann, Timmy: MI+2D+AC+TF-WeA-3, 4  
Reinert, Friedrich: MI+2D+AC+TF-WeM-1, 1  
Rogge, Paul: MI+2D+AC+TF-WeM-14, 2  
Romanova, Tetiana: AC-ThP-4, 10  
Rondinelli, James: MI+2D+AC+TF-WeM-14, 2  
Rosa, Priscila F. S.: AC+MI-ThM-3, 6  
Rosas, Debra: AC+MI-ThA-7, 8  
Roussel, Paul: AC+MI-FrM-7, **12**; AC+MI-ThA-1, 8  
Ruiz Reyes, Alberto: AC+MI-FrM-3, 12  
Russell, Daniel: MI+2D+AC+TF-WeM-8, 2  
— S —  
Sakhya, Anup Pradhan: AC-ThP-4, 10  
Schmidt, Heidemarie: MI+2D+AC+TF-WeA-10, 5  
Schneider, M. Alexander: MI+2D+AC+TF-WeM-13, 2  
Schöttke, Fabian: MI+2D+AC+TF-WeM-13, 2  
Schubert, Eva: MI+2D+AC+TF-WeA-10, 5  
Schubert, Mathias: MI+2D+AC+TF-WeA-10, 5  
Sekora, Derek: MI+2D+AC+TF-WeA-10, 5  
Servando-Williams, Donya: AC+MI-ThA-7, 8

— N —  
Narasimha, Ganesh: MI+2D+AC+TF-WeM-3, 1  
Nellis, W. J.: AC+MI-ThM-15, 7  
Neupane, Madhab: AC+MI-FrM-5, **12**; AC-ThP-4, 10  
— O —  
Orion, Itzhak: AC+MI-ThM-13, 7; AC-ThP-2, 10  
— P —  
Pantano, Gina: MI+2D+AC+TF-WeM-15, **2**  
Pearce, Charles J.: MI+2D+AC+TF-WeA-3, 4  
Peremadathil Pradeep, Reshma: MI+2D+AC+TF-WeA-11, 5  
Poudel, Narayan: AC+MI-FrM-12, 13  
Prchal, Jiri: AC+MI-FrM-8, 12  
Ptok, Andrzej: AC-ThP-4, 10  
Puggioni, Danilo: MI+2D+AC+TF-WeM-14, 2  
— R —  
Rai, Binod K.: AC+MI-FrM-13, 13  
Regmi, Paras: MI+2D+AC+TF-WeM-3, 1  
Regmi, Sabin: AC+MI-FrM-13, **13**; AC+MI-FrM-15, 13; AC-ThP-4, 10  
Reimann, Timmy: MI+2D+AC+TF-WeA-3, 4  
Reinert, Friedrich: MI+2D+AC+TF-WeM-1, 1  
Rogge, Paul: MI+2D+AC+TF-WeM-14, 2  
Romanova, Tetiana: AC-ThP-4, 10  
Rondinelli, James: MI+2D+AC+TF-WeM-14, 2  
Rosa, Priscila F. S.: AC+MI-ThM-3, 6  
Rosas, Debra: AC+MI-ThA-7, 8  
Roussel, Paul: AC+MI-FrM-7, **12**; AC+MI-ThA-1, 8  
Ruiz Reyes, Alberto: AC+MI-FrM-3, 12  
Russell, Daniel: MI+2D+AC+TF-WeM-8, 2  
— S —  
Sakhya, Anup Pradhan: AC-ThP-4, 10  
Schmidt, Heidemarie: MI+2D+AC+TF-WeA-10, 5  
Schneider, M. Alexander: MI+2D+AC+TF-WeM-13, 2  
Schöttke, Fabian: MI+2D+AC+TF-WeM-13, 2  
Schubert, Eva: MI+2D+AC+TF-WeA-10, 5  
Schubert, Mathias: MI+2D+AC+TF-WeA-10, 5  
Sekora, Derek: MI+2D+AC+TF-WeA-10, 5  
Servando-Williams, Donya: AC+MI-ThA-7, 8

— N —  
Narasimha, Ganesh: MI+2D+AC+TF-WeM-3, 1  
Nellis, W. J.: AC+MI-ThM-15, 7  
Neupane, Madhab: AC+MI-FrM-5, **12**; AC-ThP-4, 10  
— O —  
Orion, Itzhak: AC+MI-ThM-13, 7; AC-ThP-2, 10  
— P —  
Pantano, Gina: MI+2D+AC+TF-WeM-15, **2**  
Pearce, Charles J.: MI+2D+AC+TF-WeA-3, 4  
Peremadathil Pradeep, Reshma: MI+2D+AC+TF-WeA-11, 5  
Poudel, Narayan: AC+MI-FrM-12, 13  
Prchal, Jiri: AC+MI-FrM-8, 12  
Ptok, Andrzej: AC-ThP-4, 10  
Puggioni, Danilo: MI+2D+AC+TF-WeM-14, 2  
— R —  
Rai, Binod K.: AC+MI-FrM-13, 13  
Regmi, Paras: MI+2D+AC+TF-WeM-3, 1  
Regmi, Sabin: AC+MI-FrM-13, **13**; AC+MI-FrM-15, 13; AC-ThP-4, 10  
Reimann, Timmy: MI+2D+AC+TF-WeA-3, 4  
Reinert, Friedrich: MI+2D+AC+TF-WeM-1, 1  
Rogge, Paul: MI+2D+AC+TF-WeM-14, 2  
Romanova, Tetiana: AC-ThP-4, 10  
Rondinelli, James: MI+2D+AC+TF-WeM-14, 2  
Rosa, Priscila F. S.: AC+MI-ThM-3, 6  
Rosas, Debra: AC+MI-ThA-7, 8  
Roussel, Paul: AC+MI-FrM-7, **12**; AC+MI-ThA-1, 8  
Ruiz Reyes, Alberto: AC+MI-FrM-3, 12  
Russell, Daniel: MI+2D+AC+TF-WeM-8, 2  
— S —  
Sakhya, Anup Pradhan: AC-ThP-4, 10  
Schmidt, Heidemarie: MI+2D+AC+TF-WeA-10, 5  
Schneider, M. Alexander: MI+2D+AC+TF-WeM-13, 2  
Schöttke, Fabian: MI+2D+AC+TF-WeM-13, 2  
Schubert, Eva: MI+2D+AC+TF-WeA-10, 5  
Schubert, Mathias: MI+2D+AC+TF-WeA-10, 5  
Sekora, Derek: MI+2D+AC+TF-WeA-10, 5  
Servando-Williams, Donya: AC+MI-ThA-7, 8

— R —  
Rai, Binod K.: AC+MI-FrM-13, 13  
Regmi, Paras: MI+2D+AC+TF-WeM-3, 1  
Regmi, Sabin: AC+MI-FrM-13, **13**; AC+MI-FrM-15, 13; AC-ThP-4, 10  
Reimann, Timmy: MI+2D+AC+TF-WeA-3, 4  
Reinert, Friedrich: MI+2D+AC+TF-WeM-1, 1  
Rogge, Paul: MI+2D+AC+TF-WeM-14, 2  
Romanova, Tetiana: AC-ThP-4, 10  
Rondinelli, James: MI+2D+AC+TF-WeM-14, 2  
Rosa, Priscila F. S.: AC+MI-ThM-3, 6  
Rosas, Debra: AC+MI-ThA-7, 8  
Roussel, Paul: AC+MI-FrM-7, **12**; AC+MI-ThA-1, 8  
Ruiz Reyes, Alberto: AC+MI-FrM-3, 12  
Russell, Daniel: MI+2D+AC+TF-WeM-8, 2  
— S —  
Sakhya, Anup Pradhan: AC-ThP-4, 10  
Schmidt, Heidemarie: MI+2D+AC+TF-WeA-10, 5  
Schneider, M. Alexander: MI+2D+AC+TF-WeM-13, 2  
Schöttke, Fabian: MI+2D+AC+TF-WeM-13, 2  
Schubert, Eva: MI+2D+AC+TF-WeA-10, 5  
Schubert, Mathias: MI+2D+AC+TF-WeA-10, 5  
Sekora, Derek: MI+2D+AC+TF-WeA-10, 5  
Servando-Williams, Donya: AC+MI-ThA-7, 8

## Author Index

Severing, Andrea: AC+MI-ThM-3, 6; AC+MI-ThM-7, **6**  
Sharma, Peter: MI+2D+AC+TF-WeA-3, 4  
Shrestha, Ashok: MI+2D+AC+TF-WeA-4, **4**;  
MI+2D+AC+TF-WeM-7, 2; MI+2D+AC+TF-WeM-8, 2  
Shuh, David: AC+MI-ThA-6, **8**; AC+MI-ThA-7, 8  
Sinova, Jairo: MI+2D+AC+TF-WeM-15, 2  
Šmejkal, Libor: MI+2D+AC+TF-WeM-15, 2;  
MI+2D+AC+TF-WeM-5, **1**  
Smith, Arthur: MI+2D+AC+TF-WeM-7, **2**  
Smith, Arthur R.: MI+2D+AC+TF-WeA-4, 4;  
MI+2D+AC+TF-WeM-8, 2  
Smith, J. L.: AC+MI-ThM-15, 7  
Spencer, Ben: AC+MI-ThA-1, 8  
Sprague, Milo: AC-ThP-4, 10  
Srikanth, Hari: MI+2D+AC+TF-WeA-5, **5**  
stewart, Greg: AC+MI-FrM-11, **13**  
Sun, Nian Xiang: MI+2D+AC+TF-WeA-3, 4

Sundermann, Martin: AC+MI-ThM-3, 6;  
AC+MI-ThM-7, 6  
— **T** —  
Tao, Chenggang: MI+2D+AC+TF-WeM-3, 1  
Tavazohi, Pedram: MI+2D+AC+TF-WeM-4, 1  
Thareja, Eklavya: MI+2D+AC+TF-WeM-15, 2  
Tjeng, Liu Hao: AC+MI-ThM-3, **6**; AC+MI-ThM-7, 6  
Tobin, JG: AC+MI-ThA-9, **9**  
— **U** —  
Ullah, Ahsan: MI+2D+AC+TF-WeA-10, 5  
Ünzelmänn, Maximilian: MI+2D+AC+TF-WeM-1, **1**  
Upadhyay, Sneha: MI+2D+AC+TF-WeM-7, 2  
— **V** —  
Valadez, Nathan: AC-ThP-4, 10  
Valdez, Nichole R.: MI+2D+AC+TF-WeA-3, 4  
Vallejo, Keivn: AC+MI-FrM-15, **13**  
Vasudevan, Rama: MI+2D+AC+TF-WeM-3, 1

— **W** —  
Wang, Gaoxue: AC+MI-FrM-1, 12; AC+MI-FrM-14, 13  
Wang, Jiayi: MI+2D+AC+TF-WeM-14, 2  
Ward, Jesse: AC+MI-ThA-6, 8  
Ware, Washat: AC-ThP-3, **10**  
Weiss, Aryeh M.: AC+MI-ThM-13, 7; AC-ThP-2, 10  
Willcole, Alexandria: MI+2D+AC+TF-WeA-3, 4  
Wood, Aaron: AC+MI-ThA-1, 8  
Woryk, Larissa: AC-ThP-5, **10**  
— **Y** —  
Yang, Fengyuan: MI+2D+AC+TF-WeM-8, 2  
Yang, Ping: AC+MI-FrM-1, **12**; AC+MI-FrM-14, 13  
Yao, Jennifer: AC-ThP-6, **10**  
Yao, Shukai: AC+MI-FrM-14, **13**  
Yehuda-Zada, Yaacov: AC+MI-ThM-13, 7; AC-ThP-2, 10  
— **Z** —  
Zwicknagl, Gertrud: AC+MI-ThM-14, **7**